▐ **Material Science** |*Hot Paper*|

Core Halogenation as a Construction Principle in Tuning the Material Properties of Tetraazaperopyrenes

Lena Hahn,[a] Friedrich Maaß,[b] Tim Bleith,[a] Ute Zschieschang,[c] Hubert Wadepohl,[a] Hagen Klauk,[c] Petra Tegeder,[b] and Lutz H. Gade*[a]

Abstract: A detailed study on the effects of core halogenation of tetraazaperopyrene (TAPP) derivatives is presented. Its impact on the solid structure, as well as the photophysical and electrochemical properties, has been probed by the means of X-ray crystallography, UV/Vis and fluorescence spectroscopy, high-resolution electron energy loss spectroscopy (HREELS), cyclic voltammetry (CV), and DFT modeling. The aim was to assess the potential of this approach as a construction principle for organic electron-conducting materials of the type studied in this work. Although halogenation leads to a stabilization of the LUMOs compared to the unsubstituted parent compound, the nature of the halide barely affects the LUMO energy while strongly influencing the HOMO energies. In terms of band-gap engineering, it was demonstrated that the HOMO–LUMO gap is decreased by substitution of the TAPP core with halides, the effect being found to be most pronounced for the iodinated derivative. The performance of the recently reported core-fluorinated and core-iodinated TAPP derivatives in organic thin-film transistors (TFTs) was investigated on both a glass substrate, as well as on a flexible plastic substrate (PEN). Field-effect mobilities of up to 0.17 cm^2Vs^{-1} and on/off current ratio of $>10^6$ were established.

Introduction

The σ-acceptor/π-donor nature of halogen atoms in halogenated aromatic compounds governs their structure-property relationships and, consequently, their manifold applications in different fields of research. Although iodinated, chlorinated and, in particular, brominated compounds are employed as starting materials for many transformations,[1,2] fluorinated aromatics are of increasing importance in drug development due to their specific binding interactions with protein receptors.[3]

Halogenated polycyclic aromatic compounds also play an important role in the field of organic electronics, especially in the development of organic n-channel semiconducting materials possessing good stabilities in air and high electron mobilities. A strategy to obtain the required electron affinity, facilitating electron injection into the material, as well as material stability under ambient conditions,[4–14] is based on the introduction of halo-substituents, which generally lead to lower LUMO energies of molecular organic materials.[15]

Although fluorination,[16–23] chlorination,[13,15,24–26] and to some extant also bromination[12,27] of the π-conjugated systems have been shown to result in air-stable high-performing semiconductors, iodination[28–30] has been less explored to date. This might be due to the nature of the C—I bond being the weakest carbon–halogen bond. In fact, it is not unusual to observe thermal or electrochemical cleavage of carbon–iodine bonds.[15]

In recent years we developed the synthesis of 1,3,8,10-tetraazaperopyrenes (TAPP), a new class of polyheterocyclic aromatics.[31,32] TAPP derivatives have shown promising results as both fluorescence markers and organic semiconductors.[33–35] Tetrachlorinated, as well as tetrabrominated, TAPPs were demonstrated to display n-channel semiconducting behavior. Very recently, a new synthetic approach to core-functionalized TAPP derivatives via a fourfold lithiated intermediate has given access to the fourfold core fluorinated, as well as the fourfold core-iodinated, TAPP derivatives.[36] This has now provided the complete series of derivatized TAPPs displayed in Figure 1.

Herein, we present a comprehensive study into the impact of TAPP-core halogenation on the solid-state structure, the photophysical and the electrochemical behavior of these compounds, as well as a comparative study of their performance as n-channel semiconductors in thin-film transistors. In the literature, there are some examples for the comparison of fluoro-, chloro-, and to a lesser extent bromo-substituted polycyclic aromatic hydrocarbons (PAHs).[12,15,26,37] But to the best of our knowledge, a detailed investigation into structure–proper-

[a]   L. Hahn, T. Bleith, Prof. Dr. H. Wadepohl, Prof. Dr. L. H. Gade
      Anorganisch-Chemisches-Institut, Universität Heidelberg
      Im Neuenheimer Feld 270, 69120 Heidelberg (Germany)
      Fax: (+49) 6221545609
      E-mail: lutz.gade@uni-hd.de

[b]   F. Maaß, Prof. Dr. P. Tegeder
      Physikalisch-Chemisches-Institut, Universität Heidelberg
      Im Neuenheimer Feld 253, 69120 Heidelberg (Germany)

[c]   Dr. U. Zschieschang, Dr. H. Klauk
      Max Planck Institute for Solid State Research
      Heisenbergstrasse 1, 70569 Stuttgart (Germany)

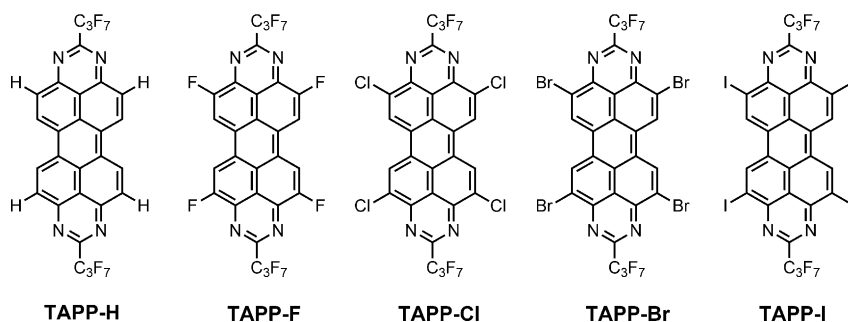⊞   Supporting information for this article is available on the WWW under
      http://dx.doi.org/10.1002/chem.201503484.

Figure 1. Overview of the molecules (**TAPP-Hal**) studied in this work.

then slightly decreases going from **TAPP-Br** to **TAPP-I**. Although the differences in the displacement perpendicular to the long molecular axis are rather pronounced, the slippage along the principal molecular axis ($\Delta_{\parallel}$) is not significantly changed upon substitution with halogens. Table 1 gives an overview of the solid-states characteristics of all halogenated TAPPs (**TAPP-Hal**).
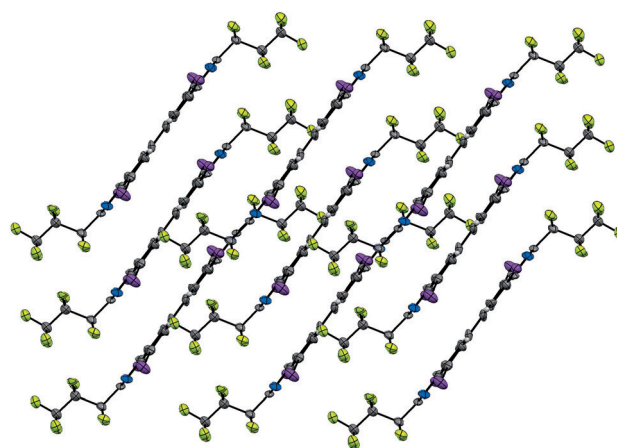
ty relationships covering the complete range of halogenated derivatives of a given molecular lead structure has not been reported to date. This has now provided new insights into the construction principles governing the development of new organic electron-conducting materials.

Results and Discussion

Solid-state structures

To allow a comparative investigation of the molecular and solid-state structures of the TAPP derivatives studied in this work, crystals of compounds **TAPP-F** and **TAPP-I** suitable for X-ray diffraction were grown from solutions in $CHCl_3$ and THF, respectively. The solid-state structures of the other three derivatives had been reported previously.[33, 34] As was observed for the unsubstituted TAPP **TAPP-H**, the fourfold chlorinated **TAPP-Cl** and fourfold brominated **TAPP-Br**, the perfluoroalkyl substituents of **TAPP-F** and **TAPP-I** are pointing in opposite directions above and below the almost planar tetraazaperopyrene core. All TAPP derivatives possess a small torsion angle of the peropyrene core.

In the case of **TAPP-F**, the crystals contain solvent molecules in the lattice, limiting the comparison of the solid structures to the ones of the other core-halogenated TAPPs in terms of packing pattern and π–π plane distance. Similar to the corresponding chlorinated and brominated TAPPs, the packing pattern of **TAPP-I** is characterized by a slip-stacked face-to-face arrangement of the molecules with a short interplanar distance of 3.39 Å, which is identical to the value observed for **TAPP-Br** (Figure 2). The substitution of hydrogen atoms by halogen atoms results in a decrease of the intermolecular distance between two neighboring molecules compared to the distance between two **TAPP-H** molecules which was found to be 3.51 Å. This observation is in agreement with the proposal that a more graphite-like structure is obtained by lowering the number of C—H bonds in polycyclic aromatic hydrocarbons.[38] We suggest, in particular, this decrease of the interplanar distance may be caused by the slippage of neighboring parallel oriented molecules (Figure 3).

This slippage of the stacks for **TAPP-H**, **TAPP-Cl**, **TAPP-Br**, and **TAPP-I** has been regarded in detail. The displacement perpendicular to the long molecular axis ($\Delta_{\perp}$) increases on going from **TAPP-H** (0.47 Å) to the chlorinated derivative (1.29 Å) and

Figure 2. Molecular packing of **TAPP-I** in the crystal. Thermal ellipsoids were drawn at 50 % probability level.
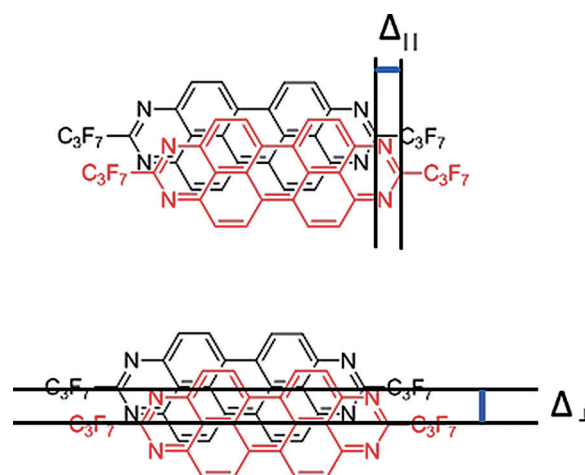

Figure 3. Stack slippage of TAPP molecules in the solid-state structure.

Adsorption of TAPP-Hal on the Au(111) surface

For the performance of small-molecule organic semiconductors in devices, the growth mechanisms on surfaces and the physical interactions at the semiconductor/metal interface are of great importance.[39] To gain some insight into the adsorption behavior, different coverages of the TAPP derivatives on the

Table 1. Overview of the crystal data of **TAPP-H** and **TAPP-Hal**.					
	TAPP-H[33]	**TAPP-F**	**TAPP-Cl**[33]	**TAPP-Br**[34]	**TAPP-I**
crystal system	triclinic	monoclinic	triclinic	triclinic	triclinic
π–π plane distance [Å]	3.51		3.38	3.39	3.39
torsion angle[a] [°]	−0.4(4)	−0.05(27)	−1.4(5)	+2.4(6)	−2.(3)
$\Delta_\perp$ [Å]	0.47		1.29	1.27	1.03
$\Delta_\parallel$ [Å]	3.39		3.37	3.43	3.58
[a] Torsion angle between the two connected naphthalene units.					

Au(111) single-crystal surface were investigated (details about the sample preparation are given in the Experimental Section). The adsorption geometries were examined by using vibrational spectroscopy, namely, angle-resolved high-resolution electron energy loss spectroscopy (HREELS).[40] HREELS has been widely used to investigate isomerization processes in molecular switches at surfaces[41] or to study 2-dimensional aromatic molecules on surfaces.[41,42]
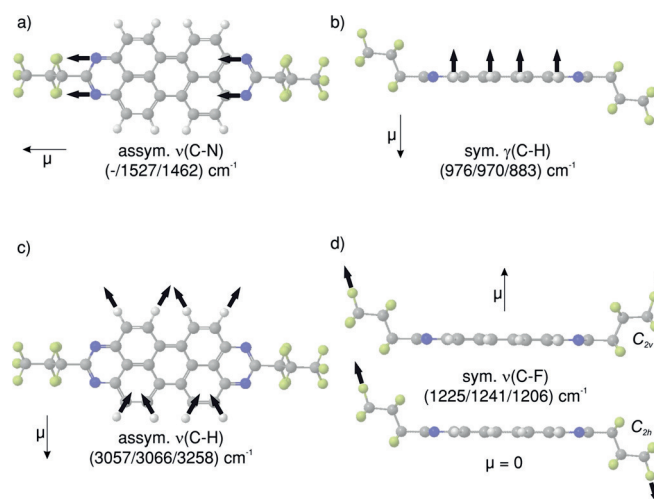
In the following, we present and discuss the data exemplarily for the **TAPP-H**. The assignment of all observed vibrational modes and the corresponding spectra for the halogenated derivatives are shown in the Supporting Information (section 1). Figure 4 shows the HREEL spectra of **TAPP-H** at a mono- (ML)
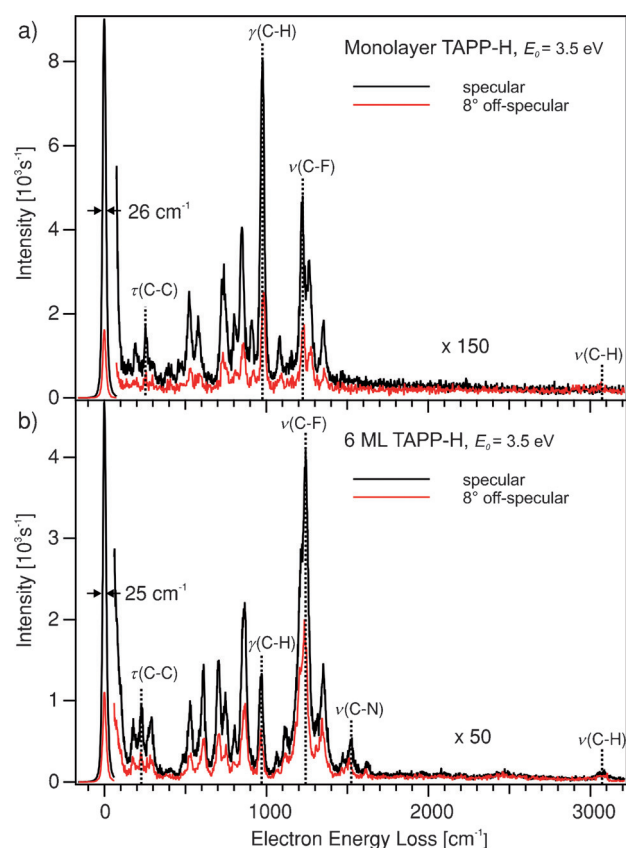
and multilayer coverage. In HREELS, monochromatic low-energy electrons hit the sample under an angle of incidence Φ_i and are scattered elastically or inelastically under an angle Φ_s. The scattered electrons are analyzed angle- and energy-resolved. There are two important scattering mechanisms, dipole and impact scattering. Long-range dipole scattering emerges from coupling of the electric field of the incoming electron (perpendicular to the surface between the electron and its image charge in the metal surface) with the part of the dynamic dipole moment of a vibration perpendicular to the surface.[40] Dipole-scattered electrons occur only in the specular direction ($\Phi_i = \Phi_s$) due to the lack of momentum transfer parallel to the surface. Short-range impact scattering is in contrast more isotropic, and the so scattered electrons can be measured in specular and off-specular ($\Phi_i \neq \Phi_s$) geometry as well. Thus, the difference between the specular (black) and off-specular (red) intensity of a loss peak in Figure 4 is a measure for its so-called dipole activity.[43] This dipole activity, again, depends strongly on the orientation of the dynamic dipole moment of the vibration with respect to the metal surface (dipole active if the projection of the vibrational dipole moment along the surface normal is large). A comparison between measured and calculated dynamic dipole moment orientations of a vibrational mode gives insight into the orientation of the molecule on the surface.

In Figure 5, important vibrational modes, as modeled by DFT (B3LYP/6-311G), are displayed with their dipole derivative unit

Figure 4. Vibrational HREEL spectra in specular (black) and off-specular (red) scattering geometry for a **TAPP-H** monolayer (a) and a coverage of 6 ML **TAPP-H** (b) on the Au(111) surface. E_0 is the primary energy of the incident electrons. The energy resolution measured as FWHM of the elastic peak (zero loss peak) is around 25 cm^{-1}.

Figure 5. Schematic visualization of calculated (DFT B3LYP/6-311G) atomic displacements (thick arrows) for the ν(C—N), γ(C—H), ν(C—H), and ν(C—F) (a–d) vibrations of TAPP-H at the declared values (HREELS monolayer/HREELS multilayer/DFT). The calculated dipole derivative unit vectors μ are shown as thin arrows.

vectors. The C—N stretching mode ν(C—N) (Figure 4a) is barely visible in the monolayer and dipole active in the multilayer (1527 cm^{-1}, Figure 4b). With its dynamic dipole moment parallel to the long axis of the molecule, we can draw the conclu-

sion that the aromatic backbones of the molecules in the ML regime lie flat on the surface. In the multilayer, they are tilted around their short axes, a finding which is supported by the reduced dipole activity and the reduced relative intensity of the out-of-plane C−H bending mode γ(C−H) in the multilayer (970 cm^{-1}, Figure 4b) compared to the monolayer (976 cm^{-1}, Figure 4a). The tilting of the molecule implies a tilt in the dynamic dipole moment of the respective vibration and accordingly reducing the component perpendicular to the surface. The almost invisible C−H stretching mode ν(C−H) at 3057 cm^{-1} (Figure 4a) and 3066 cm^{-1} (Figure 4b) with its dynamic dipole moment parallel to the short axis of the molecule (Figure 5c) indicates that the dipole is compensated by the image dipole of the metal surface. The latter is the case if the molecule is not tilted around its long axis in the mono- and multilayer regime. The different vibrational modes associated with the perfluorinated side chains are located in the same energy regime (1100 to 1400 cm^{-1}), thus precluding an unambiguous assignment. Geometrical arguments let us conclude that the side chains point upwards in the monolayer to reduce the distance between the aromatic molecular backbone and the metal surface allowing for increased attractive interactions. The spectra depicted in Figure 4 show distinct differences between the mono- and the multilayer. We assign these differences to the different orientation of the side chains, which changes the symmetry of the molecule from C_{2v} (monolayer) to C_{2h} (multilayer; see Figure 5d). This change leads to a different dipole activity of the involved modes (ν(C−F) at 1225 and 1241 cm^{-1} in Figure 4a and b, respectively). Several different coverages were studied, and all the mentioned changes occurred between a coverage of one and two ML, and no additional changes were observed when going to higher coverages. We therefore conclude that the different orientation takes place immediately after reaching a coverage of one ML.

In Figure 6, structural models for the adsorption behavior of the different TAPP derivatives on the Au(111) surface are pre-
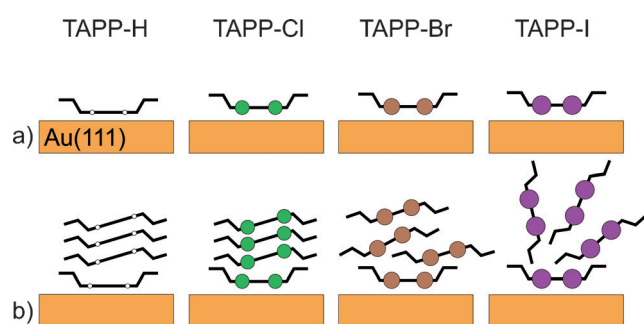
Figure 6. Developed model for the adsorption geometries in the mono- (a) and multilayer (b) regimes for the different TAPP derivatives on Au(111).

sented (all relevant spectra and analyses can be found in the Supporting Information, section 1). The **TAPP-H**, **TAPP-Cl**, **TAPP-Br**, and **TAPP-I** monolayers are well ordered, with a flat-lying aromatic system and perfluorinated side-chains pointing "upwards" (Figure 6a). The **TAPP-H** and **TAPP-Cl** multilayers are

also well ordered, tilted around the short axis, with a short axis parallel to the surface, and the side-chains point in opposite directions (Figure 6b). The **TAPP-Br**, and even more so the iodinated derivative **TAPP-I**, give rise to less ordered multilayers, which is manifested in broadened loss peaks, reduced dipole activity, and a reduced intensity of the elastic peak. We conclude that the effect of the metallic substrate on the film growth is strongly reduced from the second layer onwards. For higher coverages, the molecules adopt the crystal-like orientation.

Photophysical and electrochemical properties in solution

For the applicability of a molecular organic compound as an organic semiconductor, the energies of the frontier orbitals are key parameters. In electron-conducting organic semiconducting materials, the charge transport occurs predominantly by electron hopping through low-lying LUMOs, with LUMO energies of less than −3.7 eV being considered essential for an efficient electron transport according to the literature.[44] The molecular electronic properties can be experimentally probed by cyclic voltammetry (CV), as well as UV/Vis absorption spectroscopy or similar methods. Furthermore, we employed a B3LYP[45–47]/def2-SVP[48]//B3LYP/def2-QZVPP[49] computational tool implemented in the ORCA modelling package[50] to predict properties that are difficult to determine experimentally.

In general, σ-acceptors lead to a stabilization of HOMO and LUMO, whereas π-donors destabilize the frontier orbitals; however, the latter strongly depends on the orbital coefficients on the substituents. Comparing the energy levels of the frontier orbitals of **TAPP-H** with those of **TAPP-Hal** reflects the σ-acceptor and π-donor duality of the halogen substituents. The calculated LUMO levels, which were found in the range of −4.1 to −3.9 eV for **TAPP-Hal**, experience a significant stabilization of around 0.4 eV compared to **TAPP-H**, as was expected for substitution with more electronegative halogen atoms (Table 2).

Because there is only minor (orbital) contribution of the halide to the respective LUMO π-orbital (see Figure 7), the nature of the halide has a negligible effect on the LUMO energies themselves. However, as displayed in Figure 7, there is a strong contribution of the halide to the HOMO π-orbitals, which increases upon going from **TAPP-F** to **TAPP-I**. Overall, this leads to an expansion of the π-system and an increase in the HOMO energies, and thus a reduction in the HOMO–LUMO gaps in this series (Figure 8).

Experimental determination of LUMO levels using CV (according to literature methods using Fc/Fc$^+$ as an internal standard, setting E_{HOMO}(Fc) = −4.8 eV) showed a very good agreement with the calculated data (Table 2). Moreover, the calculated electron affinities are around 3 eV, indicating potential n-channel semiconductor behavior for the **TAPP-Hal** derivatives (see above), and heavy-element substitution increases electron affinities considerably up to 3.13 eV.
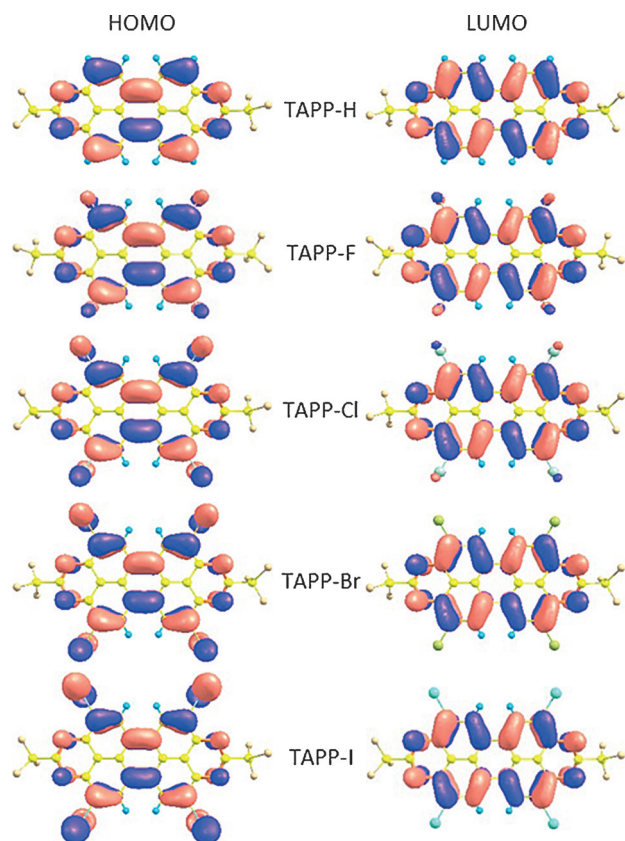
Figure 9 shows the characteristic absorption maxima of the π*←π transition of all **TAPP-Hal** derivatives, as well as the parent compound **TAPP-H** recorded in THF. Halogenation of

| Table 2. Electrochemical and calculated properties of the TAPP derivatives.						
	E_{Red1}[a] [V]	E_{Red2}[a] [V]	$E_{LUMO (CV)}$[b] [eV]	$E_{HOMO (DFT)}$[c] [eV]	$E_{LUMO (DFT)}$ [eV]	$EA_{(DFT)}$ [eV]
TAPP-H				−6.61	−3.66	2.62
TAPP-F	−0.32	−0.76	−3.92	−6.69	−3.93	2.97
TAPP-Cl	−0.18	−0.59	−4.06	−6.62	−3.99	3.09
TAPP-Br	−0.18	−0.56	−4.04	−6.61	−4.02	3.13
TAPP-I	−0.22	−0.57	−4.02	−6.51	−4.00	3.11

[a] Measured against SCE in THF. [b] Determined according to literature methods by using Fc/Fc$^+$ as an internal standard (E_{HOMO}(Fc) = −4.8 eV).[51] [c] Calculated at the B3LYP/def2-SVP//B3LYP/def2-QZVPP level of theory.

Cl displays the highest fluorescence quantum yield (φ_{Em} = 0.78), whereas **TAPP-Br** (φ_{Em} = 0.12) and **TAPP-I** (φ_{Em} = 0.02) were found to be only weakly fluorescent, and the fluorescence lifetimes almost entirely dominated by the non-radiative relaxation (τ_{nonrad}, Table 3). We attribute this fact to the presence of the heavy atoms bromine and iodine, respectively, resulting in fluorescence quenching (internal heavy atom effect) due to an increased probability of intersystem crossing.

Figure 7. Frontier orbitals of TAPP-derivatives **TAPP-H–TAPP-I**, isoval. = 0.03.
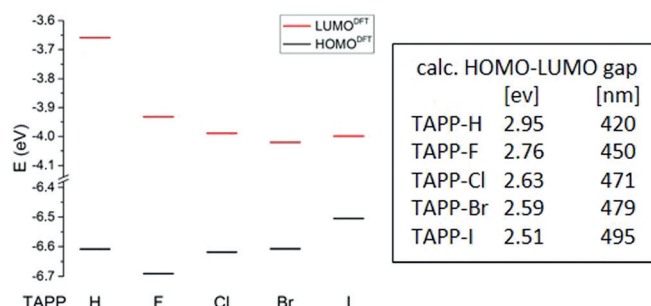
Figure 8. Overview of the calculated HOMO and LUMO energies of TAPP-derivatives **TAPP-H** and **TAPP-Hal**.

Electronic structure of TAPP-Hal in thin films

A complementary method to UV/VIS absorption spectroscopy is electronic HREELS. This surface-sensitive method gives insight into the electronic structure of adsorbed molecules, which is needed for an understanding of their properties at surfaces and interfaces, because they appear as important junctions in organic molecule-based devices. Electronic HREELS has been successfully applied to study organic semiconductors[42,52,53] and graphene nanoribbons[54,55] on noble metal surfaces. It allows, amongst others, the determination of optical gaps by exciting intramolecular electronic transitions from the ground state (S$_0$, HOMO) to the excited state (e.g., S$_1$, LUMO).

In Figure 10, the electronic HREEL spectra for the **TAPP-H**, **TAPP-Cl**, **TAPP-Br**, and **TAPP-I** adsorbed on the Au(111) surface are displayed. To eliminate potential surface plasmon modes of the substrate and to render the situation closer to that encountered in real devices, multilayer coverages were measured (4–5 monolayers, determined by thermally programmed desorption). The vibronic transitions have been fitted with Gaussian fit functions. The peak positions of the three halogenated

the TAPP core leads to a bathochromic shift of the absorption maximum compared to the unsubstituted analogue in the order F < Cl < Br < I, mirroring the successive rise in the HOMO energies represented in Figure 8. Comparison of the experimentally measured spectra to the spectral transitions simulated using time-dependent (TD) DFT showed that except for a slight overestimation of excitation energies, TDDFT predicts the positions of the absorption bands with satisfactory accuracy. All halogenated TAPPs are fluorescent in solution (Figure 9). The chlorinated derivative **TAPP-**

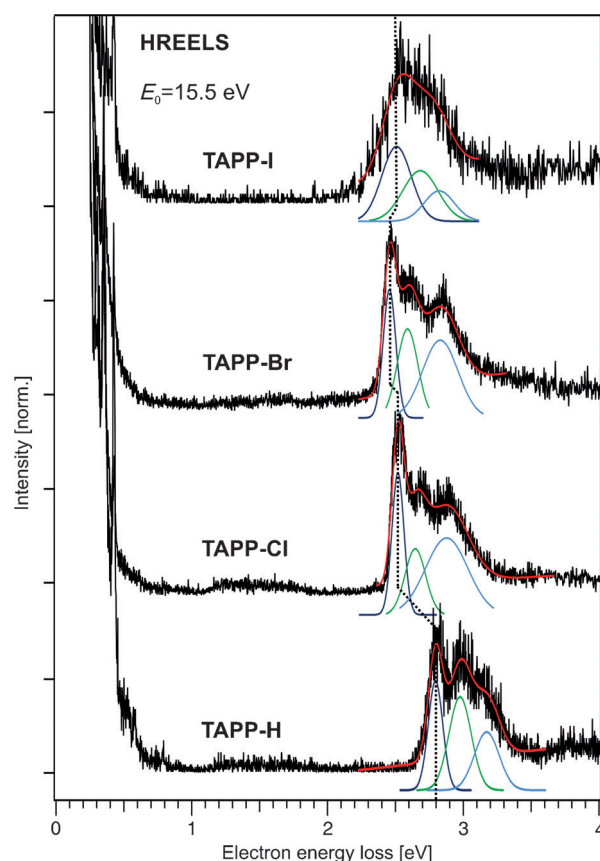| Table 3. Photophysical properties of the TAPP derivatives; τ = lifetimes (total, radiative, non-radiative).							
	λ_{max} [nm] (log ε)	$\Delta\tilde{\nu}$ [cm^{-1}]	λ_{em} [nm]	Φ_{em}	$\lambda_{max(DFT)}$ [nm]	τ_{tot} [ns]	τ_{rad} [ns]	τ_{nonrad} [ns]
TAPP-H	436 (4.50)	1454	448	0.51	408	3.10	6.08	6.32
TAPP-F	453 (4.82)	1356	471	0.68	430	2.90	4.26	9.08
TAPP-Cl	469 (4.89)	1405	479	0.78	448	2.40	3.08	10.87
TAPP-Br	475 (4.91)	1419	486	0.12	458	0.43	3.58	0.48
TAPP-I	494 (4.93)	1455	518	0.02	485	0.24	12.0	0.24
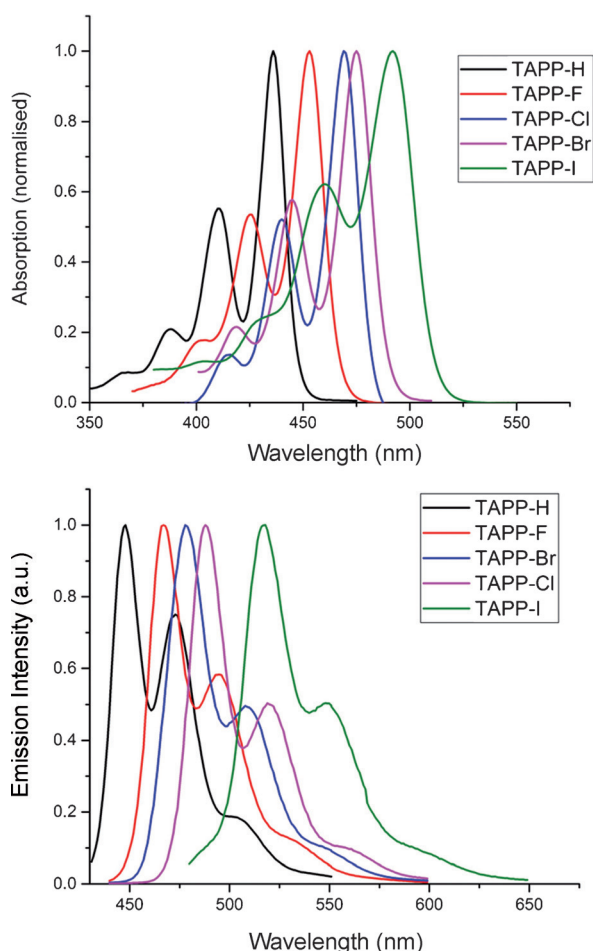
Figure 9. UV/Vis spectra of the five **TAPP** compounds, recorded in THF (top). Emission spectra of the five TAPP compounds, recorded in THF (bottom).

Figure 10. Electronic HREEL spectra for multilayer coverages of three halogenated and the unsubstituted TAPP derivatives with fits to the vibronic S_0–S_1 transition peaks. The primary electron energy is 15.5 eV and the spectra are normalized with respect to the S_0–S_1 transition peak (dashed line).

species are identical within experimental error (**TAPP-Cl** 2.49 ± 0.06 eV; **TAPP-Br** 2.42 ± 0.06 eV; **TAPP-I** 2.48 ± 0.15 eV) and lie 0.3 eV below the unsubstituted parent compound **TAPP-H** (2.77 ± 0.07 eV). The **TAPP-I** spectrum possesses a low signal-to-noise ratio due to the disordered molecular adsorption when going to coverages above one monolayer, as described above and in the Supporting Information (section 1.4).

The vibration involved in the vibronic transitions is the C–N stretching mode located at 1450 cm^{-1}.[33] As expected, in the multilayer regime the influence of the metal substrate on the optical gap size is negligible, thus, the values obtained from UV/Vis and HREELS are similar (for **TAPP-Cl**: 2.64 eV, UV/VIS in THF;[33] 2.49 ± 0.06 eV, electronic HREELS). However, no variation of the gap size due to the value of the halogen substituent was observed. In contrast, a pronounced decrease is found when substituting the **TAPP-H** parent compound: the gap decreases by 0.28 ± 0.09 eV (UV/Vis 0.2 eV)

Fabrication of organic transistors

It has been shown in recent years that organic n-channel thin-film transistors fabricated with TAPP derivatives as semiconducting material can be operated under ambient conditions.

These devices displayed excellent long-term stability with field-effect mobility of up to 0.14 cm^{2}V^{-1}s^{-1}, which was observed for **TAPP-Cl**.[33] The core-brominated TAPP derivative **TAPP-Br** was also successfully employed in thin-film transistors; however, the highest electron mobility found for **TAPP-Br** (0.032 cm^{2}V^{-1}s^{-1}) was about four times lower than found for the chlorinated derivative.[34] In this work, the potential of TAPP derivatives **TAPP-F** and **TAPP-I** for transistor applications was evaluated in bottom-gate, top-contact TFTs. Electron mobilities (μ_n, determined in the saturation regime), on/off current ratios (I_{on}/I_{off}), subthreshold swings (SS), and threshold voltages (V_{th}) were extracted from the current/voltage characteristics.[56] Figure 11 displays the schematic cross-sections of the TFTs fabricated in this work. Although the fluorinated TAPP derivative **TAPP-F** was found to possess a rather low electron mobilities of 0.007 cm^{2}V^{-1}s^{-1} on a silicon substrate and 0.0001 cm^{2}V^{-1}s^{-1} on a flexible polyethylene naphthalate substrate (PEN) (Figure 12), for TFTs fabricated with **TAPP-I** an electron mobility of 0.17 cm^{2}V^{-1}s^{-1} in TFTs on silicon substrates and 0.06 cm^{2}V^{-1}s^{-1} in TFTs on flexible PEN substrates were observed (Figure 13).

Unexpectedly, the best performance out of all TFTs fabricated from core-halogenated TAPPs was therefore found for the iodinated TAPP derivative **TAPP-I** with an electron mobility of 0.17 cm^{2}V^{-1}s^{-1}. This is an interesting observation considering
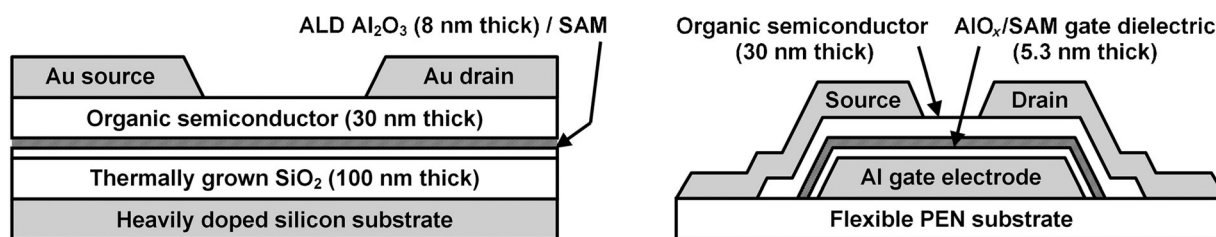
Figure 11. Schematic cross-sections of the TFTs. Left: The substrate is a heavily doped silicon wafer that also serves as the gate electrode, and the gate dielectric is a combination of 100 nm-thick thermally grown SiO_2, 8 nm-thick Al_2O_3 deposited by atomic layer deposition (ALD) and a tetradecylphosphonic acid self-assembled monolayer (SAM). Right: The substrate is flexible polyethylene naphthalate (PEN; 125 nm thick) and the gate dielectric is a combination of a 3.6 nm-thick layer of oxygen-plasma-grown AlO_x and a tetradecylphosphonic acid SAM. The gate electrodes, the semiconductor layer, and the source and drain contacts are patterned using shadow masks.
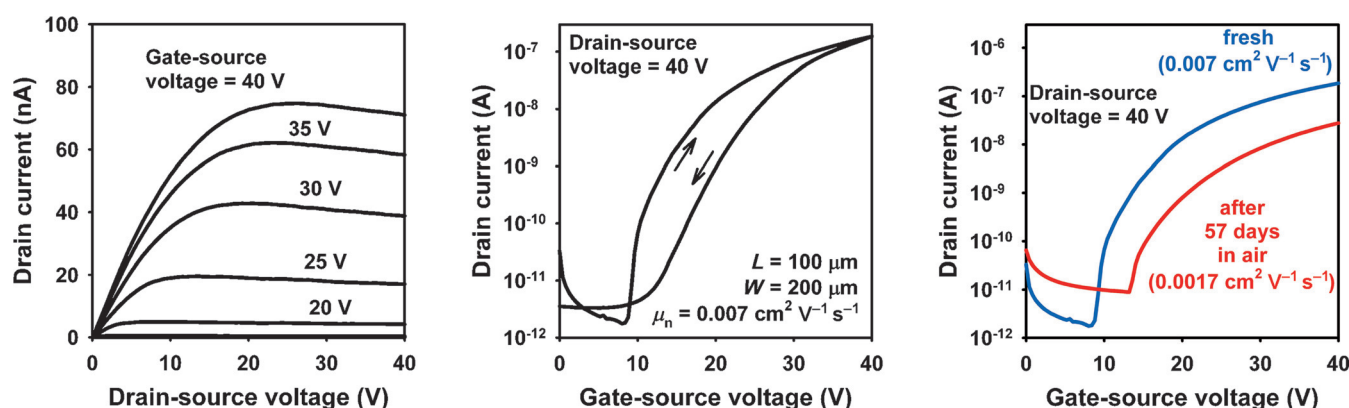
Figure 12. Current/voltage characteristics of a TFT with a vacuum-deposited layer of **TAPP-F** as the semiconductor. The substrate is a heavily doped silicon wafer and the gate dielectric is SiO_2/Al_2O_3/SAM with a total thickness of 110 nm.

that not much attention has been devoted to iodinated polycyclic aromatic hydrocarbons. We attribute the latter to the fact that in many cases, the stability of the carbon-iodine bond is a limiting factor when it comes to the application of iodinated polycyclic aromatics in organic electronics.

However, in the case of **TAPP-I**, no signs of decomposition or loss of iodine were observed after sublimation at temperatures higher than 100 °C. The long-term air stability of TFT fabricated with **TAPP-F** and **TAPP-I** was monitored by storing the TFTs in ambient air for 57 and 62 days, respectively. Whilst the electron mobility of **TAPP-F** dropped to 0.0017 cm²V⁻¹s⁻¹, the corresponding value found for **TAPP-I** was found to be 0.04 cm²V⁻¹s⁻¹. This demonstrates that the electron mobility of

TFTs based on **TAPP-I** is relatively stable during the course of prolonged air exposure. All parameters observed from TFTs fabricated with the four halogenated TAPPs and the non-halogenated **TAPP-H**, respectively, are summarized in Table 4.

Transfer integrals for the intermolecular charge transfer and influence of the thin-film morphology

When attempting to predict the suitability of an organic molecule as n-type semiconductor, the LUMO energy, the electron affinity, the π–π plane distance, as well as the transfer integrals of the organic compound, are important factors. Table 5 gives an overview of these data for **TAPP-H** and **TAPP-Hal**, as well as

Table 4. Summary of the transistor parameters electron field-effect mobility (μ_n), on/off current ratio (I_{on}/I_{off}), threshold voltage (V_{th}) and subthreshold swing (SS) measured in ambient air.

| | Ref. | TFTs on silicon substrates with thick SiO_2/Al_2O_3/SAM gate dielectric | | | | TFTs on glass or flexible PEN substrates with thin AlO_x/SAM gate dielectric | | | |
		μ_n [cm²V⁻¹s⁻¹]	I_{on}/I_{off}	V_{th} [V]	SS [V dec⁻¹]	μ_n [cm²V⁻¹s⁻¹]	I_{on}/I_{off}	V_{th} [V]	SS [V dec⁻¹]
TAPP-H	[33]	0.05	10^5	29	2.0	0.03[b]	10^3	2.1	0.27
TAPP-F	this work	0.007	6×10^4	15	3.2	0.0001[a]	10^3	0.6	0.60
TAPP-Cl	[33]	0.14	10^6	22	2.0	0.035[b]	10^5	1.7	0.25
TAPP-Br	[34]	0.032	5×10^5	18	1.8	0.017[a]	10^5	1.1	0.22
TAPP-I	this work	0.17	10^6	14	1.3	0.06[a]	5×10^5	0.6	0.10

[a] TFTs on flexible PEN substrate. [b] TFTs on glass substrate.
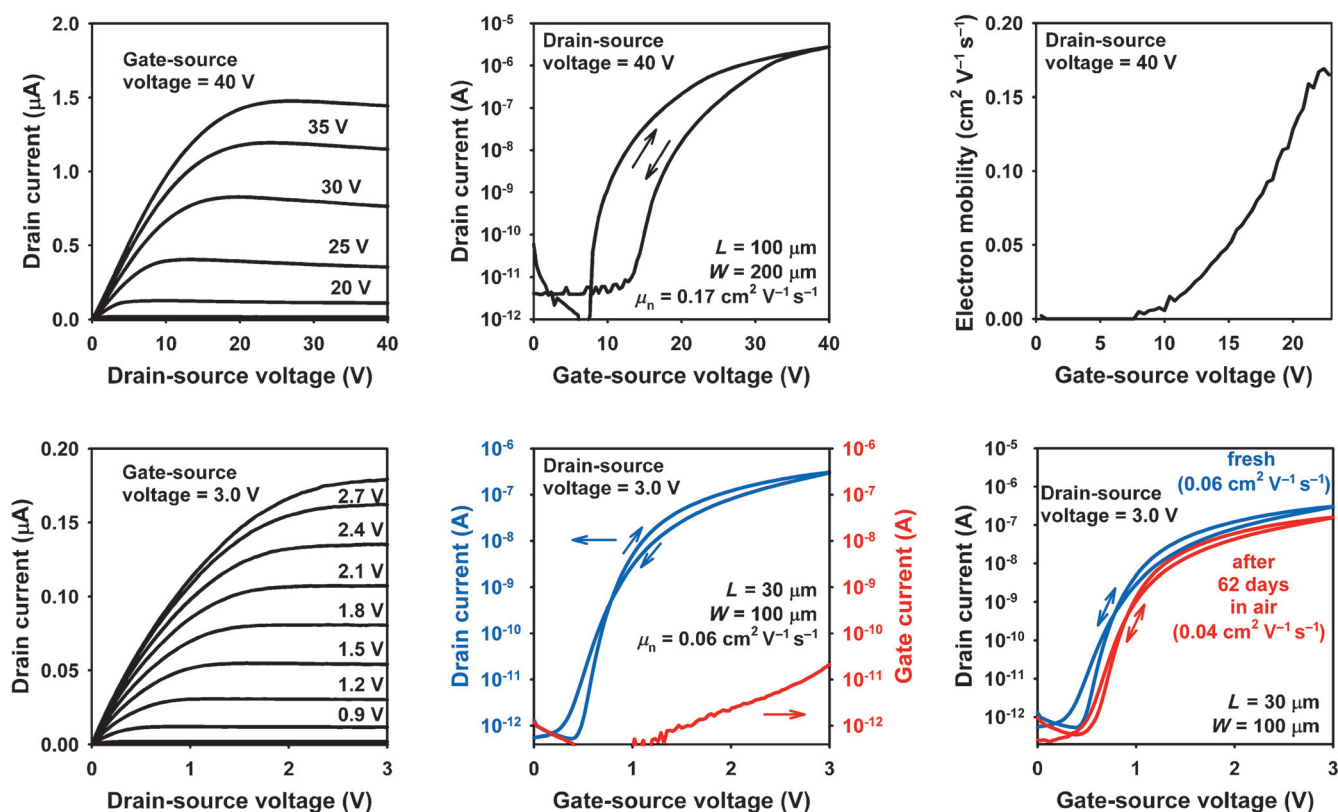
Figure 13. Current/voltage characteristics of TFTs with a vacuum-deposited layer of **TAPP-I** as the semiconductor. Top: The substrate is a heavily doped silicon wafer and the gate dielectric is $SiO_2/Al_2O_3/SAM$ with a total thickness of 110 nm. Bottom: The substrate is flexible polyethylene naphthalate (PEN) and the gate dielectric is AlO_x/SAM with a total thickness of 5.3 nm.

**Table 5.** Comparison of predictive n-type semiconductor properties and electron mobility of compounds **TAPP-H** and **TAPP-Hal**.

	E_{LUMO} [eV]	$EA_{(DFT)}$ [eV]	$\pi-\pi$ plane distance [Å]	Transfer integral (t) [meV]	μ_n [$cm^2 V^{-1} s^{-1}$]
TAPP-H	-3.66[a]	2.62	3.51	51	0.05
TAPP-F	-3.92	2.97	–	–	0.007
TAPP-Cl	-4.06	3.09	3.38	84	0.14
TAPP-Br	-4.04	3.13	3.39	109	0.032
TAPP-I	-4.02	3.11	3.39	144	0.17

their electron mobility. The carrier mobility in crystalline organic semiconductors can roughly be assessed using Marcus theory. To evaluate the required transfer integrals t, the $\pi-\pi$ overlap of a **TAPP** dimer was calculated using the projective method by Kirkpatrick,[57,58] and the results are shown in Table 5. The transfer integrals increase going from **TAPP-H** to **TAPP-I**, which is most probably due to the increasing van der Waals radii in the following order $H < Cl < Br < I$ and decrease in $\pi-\pi$ interplane distance.

Overall, the data shown in Table 5 are in good agreement with the (observed) increase in electron mobility on going from **TAPP-H** to **TAPP-Cl** and to **TAPP-I**; however, the data also suggest that the electron mobility of **TAPP-Br** should be higher than that found for **TAPP-H** and **TAPP-Cl**. Therefore, the

comparatively low electron mobility of **TAPP-Br** had to be explained by the surface morphology of the organic film in the fabricated device. Figure 14 shows AFM images of the transistors surfaces fabricated with **TAPP-Br** (left) and **TAPP-I** (right) as semiconductor. Although both AFM images of the TFT show a crystalline surface, in the case of **TAPP-Br**, cracks are observable in the surface structure. Attempts to vary the substrate temperature led to the same results. This morphological effect may result in the rather low observed electron mobility of **TAPP-Br** compared to **TAPP-Cl** and **TAPP-I**, and therefore suggests that this might be caused by its processabilty rather than its intrinsic properties.
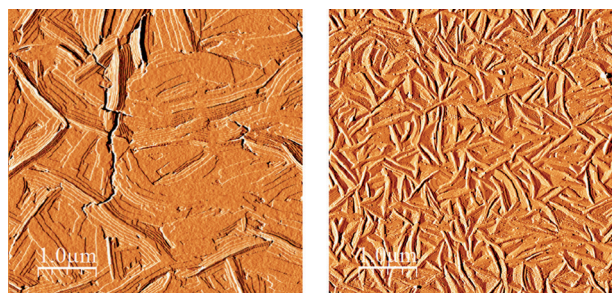
Figure 14. AFM image of an OFET fabricated with TAPP-Br (left) and TAPP-I (right) as n-type semiconductor.

Conclusion

We have presented a detailed study on the impact of core halogenation of tetraazaperopyrenes on the photophysical, as well as the electrochemical properties, to assess its potential as a construction principle for organic electron-conducting materials of the type studied in this work. In terms of band-gap engineering, it was demonstrated that the HOMO–LUMO gap is decreased by substitution of the TAPP core with halides, the effect being found to be most pronounced for the iodinated derivative **TAPP-I**. Although halogenation leads to a stabilization of the LUMOs compared to the unsubstituted parent compound, the nature of the halide barely affects the LUMO energy while strongly influencing the HOMO energies.

In terms of crystal engineering, the packing pattern remains the same, as was found for the unsubstituted parent compound suggesting a stronger influence of the perfluoroalkyl group in the 2,9-position rather than the nature of the monoatomic core substituent. However, a decrease in the π–π interplanar distance was observed upon halogenation.

Angle-resolved HREELS measurements, which were carried out to obtain information about the growth of the TAPP derivatives on a Au(111) surface, suggest that the surface-induced effect on the film growth vanishes already in the second layer. For the following layers similar molecular orientation was observed, as found in the solid molecular structures.

It has been shown in recent years that not only fluorinated but also chlorinated and brominated molecules are useful materials in terms of electron transport and device stability. We found that all halogenated TAPP derivatives exhibit n-channel semiconducting properties. Whereas the fluorinated derivative **TAPP-F** possesses the lowest electron mobility, we found that the iodinated derivative **TAPP-I** gives the best electron mobility of 0.17 cm^{2}V^{-1}s^{-1}, which is the highest value of all TAPPs fabricated in TFTs so far. This result suggests that iodinated polycyclic aromatic compounds should not be dismissed when looking for n-type organic semiconducting materials. To the best of our knowledge, this has been the first comparison of the full range of halogenated derivatives of one type of compound giving useful insights into the effect of core halogenation.

Experimental Section

All TAPP derivatives (**TAPP-H**, **TAPP-Hal**) were synthesized according to literature procedures.[33,34,36] Crystals suitable for X-ray diffraction of **TAPP-F** were obtained from a concentrated solution of **TAPP-F** in CDCl$_3$, whereas crystals of **TAPP-I** were obtained from a concentrated solution of **TAPP-I** in THF.

X-ray crystal-structure determinations: Crystal data and details of the structure determinations of compound **TAPP-F** and **TAPP-I** are listed in the Supporting Information.

HREELS measurements: The high-resolution electron energy loss spectra were recorded with a commercial SPECS Delta 0.5 HREEL spectrometer, with primary electron energies E_0 of 3.5 eV and 15 eV for the vibrational and electronic spectra, respectively. The measurements were carried out under ultra-high vacuum conditions (base pressure: 1×10^{-10} mbar). A clean Au(111) surface was prepared by repeated Ar$^+$ sputtering and annealing cycles (at 750 K). TAPP derivatives were evaporated from a home-built effusion cell held at 450 K and a substrate temperature of 300 K. The dosing was monitored with a quadrupole mass spectrometer (QMS), which was also used to determine the coverage by thermal programmed desorption (TPD). The assignment of vibrational modes is based on gas-phase DFT calculations carried out with the Gaussian 09 package.[63] Optimization of the molecular geometry and calculation of the vibrational frequencies for the free molecules were carried out with the B3LYP/6-311G tool.

Computational details: The DFT calculations were carried out using ORCA 3.0.1 program package.[50] B3LYP was employed as functional;[45–47] a def2-SVP basis set was used for all atoms during geometry optimizations and for calculations of HOMO and LUMO energies.[48] For iodine atoms, a the corresponding pseudopotential[59] was employed as implemented in ORCA 3.0.1. All other properties were calculated using a def2-QZVPP basis set.[49] A COSMO solvation model[60,61] (solvent THF: $\varepsilon = 7.25$, refractive index $= 1.407$) was applied additionally for the TDDFT calculations, the first 20 excitations of which were calculated and triplets were not allowed. Adiabatic electron affinities were calculated by comparison of the def2-QZVPP-single point energies at def2-SVP-optimized structures of the neutral molecule and the radical anion, respectively. Visualization of orbitals was done using ChemCraft.[62] Coordinates of the optimized structures can be found in the Supporting Information.

[1] K. C. Nicolaou, P. G. Bulger, D. Sarlah, *Angew. Chem. Int. Ed.* **2005**, *44*, 4442 – 4489; *Angew. Chem.* **2005**, *117*, 4516 – 4563.

[2] J. F. Hartwig, *Angew. Chem. Int. Ed.* **1998**, *37*, 2046 – 2067; *Angew. Chem.* **1998**, *110*, 2154 – 2177.

[3] K. Müller, C. Faeh, F. Diederich, *Science* **2007**, *317*, 1881 – 1886.

[4] B. A. Jones, A. Facchetti, M. R. Wasielewski, T. J. Marks, *J. Am. Chem. Soc.* **2007**, *129*, 15259 – 15278.

[5] B. A. Jones, M. J. Ahrens, M.-H. Yoon, A. Facchetti, T. J. Marks, M. R. Wasielewski, *Angew. Chem. Int. Ed.* **2004**, *43*, 6363 – 6366; *Angew. Chem.* **2004**, *116*, 6523 – 6526.

[6] R. T. Weitz, K. Amsharov, U. Zschieschang, E. B. Villas, D. K. Goswami, M. Burghard, H. Dosch, M. Jansen, K. Kern, H. Klauk, *J. Am. Chem. Soc.* **2008**, *130*, 4637–4645.

[7] U. Zschieschang, K. Amsharov, R. T. Weitz, M. Jansen, H. Klauk, *Synth. Met.* **2009**, *159*, 2362–2364.

[8] Z. Bao, A. J. Lovinger, J. Brown, *J. Am. Chem. Soc.* **1998**, *120*, 207–208.

[9] H. E. Katz, J. Johnson, A. J. Lovinger, W. Li, *J. Am. Chem. Soc.* **2000**, *122*, 7787–7792.

[10] J. Mei, Y. Diao, A. L. Appleton, L. Fang, Z. Bao, *J. Am. Chem. Soc.* **2013**, *135*, 6724–6746

[11] H. Z. Chen, M. M. Ling, X. Mo, M. M. Shi, M. Wang, Z. Bao, *Chem. Mater.* **2007**, *19*, 816–824.

[12] R. Schmidt, J. H. Oh, Y.-S. Sun, M. Deppisch, A.-M. Krause, K. Radacki, H. Braunschweig, M. Könemann, P. Erk, Z. Bao, F. Würthner, *J. Am. Chem. Soc.* **2009**, *131*, 6215–6228.

[13] J. H. Oh, S. Suraru, W.-Y. Lee, M. Könemann, H. W. Höffken, C. Röger, R. Schmidt, Y. Chung, W.-C. Chen, F. Würthner, Z. Bao, *Adv. Funct. Mater.* **2010**, *20*, 2148–2156.

[14] M. Gsänger, J. H. Oh, M. Könemann, H. W. Höffken, A.-M. Krause, Z. Bao, F. Würthner, *Angew. Chem. Int. Ed.* **2010**, *49*, 740–743; *Angew. Chem.* **2010**, *122*, 752–755.

[15] M. L. Tang, Z. Bao, *Chem. Mater.* **2011**, *23*, 446–455.

[16] A. Facchetti, M.-H. Yoon, C. L. Stern, H. E. Katz, T. J. Marks, *Angew. Chem. Int. Ed.* **2003**, *42*, 3900–3903; *Angew. Chem.* **2003**, *115*, 4030–4033.

[17] R. Schmidt, M. M. Ling, J. H. Oh, M. Winkler, M. Könemann, Z. Bao, F. Würthner, *Adv. Mater.* **2007**, *19*, 3692–3695.

[18] Y. Ie, Y. Umemoto, M. Okabe, T. Kusunoki, K. Nakayama, Y.-J. Pu, J. Kido, H. Tada, Y. Aso, *Org. Lett.* **2008**, *10*, 833–836.

[19] S. Salman, M. C. R. Delgado, V. Coropceanu, J.-L. Brédas, *Chem. Mater.* **2009**, *21*, 3593–3601.

[20] F. Babudri, G. M. Farinola, F. Naso, R. Ragni, *Chem. Commun.* **2007**, 1003–1022.

[21] M. C. R. Delgado, K. R. Pigg, D. A. da Silva Filho, N. E. Gruhn, Y. Sakamoto, T. Suzuki, R. M. Osuna, J. Casado, V. Hernández, J. T. L. Navarrete, N. G. Martinelli, J. Cornil, R. S. Sánchez-Carrera, V. Coropceanu, J.-L. Brédas, *J. Am. Chem. Soc.* **2009**, *131*, 1502–1512.

[22] Y. Sakamoto, T. Suzuki, M. Kobayashi, Y. Gao, Y. Fukai, Y. Inoue, F. Sato, S. Tokito, *J. Am. Chem. Soc.* **2004**, *126*, 8138–8140.

[23] Y. Sakamoto, S. Komatsu, T. Suzuki, *J. Am. Chem. Soc.* **2001**, *123*, 4643–4644.

[24] A. M. Hiszpanski, J. D. Saathoff, L. Shaw, H. Wang, L. Kraya, F. Lüttich, M. A. Brady, M. L. Chabinyc, A. Kahn, P. Clancy, Y.-L. Loo, *Chem. Mater.* **2015**, *27*, 1892–1900.

[25] C.-L. Song, C.-B. Ma, F. Yang, W.-J. Zeng, H.-L. Zhang, X. Gong, *Org. Lett.* **2011**, *13*, 2880–2883.

[26] F. Paulus, B. D. Lindner, H. Reiß, F. Rominger, A. Leineweber, Y. Vaynzof, H. Sirringhaus, U. H. F. Bunz, *J. Mater. Chem. C* **2015**, *3*, 1604–1609.

[27] T. Okamoto, M. L. Senatore, M.-M. Ling, A. B. Mallik, M. L. Tang, Z. Bao, *Adv. Mater.* **2007**, *19*, 3381–3384.

[28] E. Mete, D. Uner, M. Çakmak, O. Gulseren, Ş. Ellialtoglu, *J. Phys. Chem. C* **2007**, *111*, 7539–7547.

[29] R. S. Sánchez-Carrera, S. A. Odom, T. L. Kinnibrugh, T. Sajoto, E.-G. Kim, T. V. Timofeeva, S. Barlow, V. Coropceanu, S. R. Marder, J.-L. Brédas, *J. Phys. Chem. B* **2010**, *114*, 749–755.

[30] B. Ellman, S. Nene, A. N. Semyonov, R. J. Twieg, *Adv. Mater.* **2006**, *18*, 2284–2288.

[31] T. Riehm, G. De Paoli, A. E. Konradsson, L. De Cola, H. Wadepohl, L. H. Gade, *Chem. Eur. J.* **2007**, *13*, 7317–7329.

[32] a) S. C. Martens, T. Riehm, S. Geib, H. Wadepohl, L. H. Gade, *J. Org. Chem.* **2011**, *76*, 609–617; b) S. Geib, S. C. Martens, M. Märken, A. Rybina, H. Wadepohl, L. H. Gade, *Chem. Eur. J.* **2013**, *19*, 13811–13822.

[33] S. C. Martens, U. Zschieschang, H. Wadepohl, H. Klauk, L. H. Gade, *Chem. Eur. J.* **2012**, *18*, 3498–3509.

[34] S. Geib, U. Zschieschang, M. Gsänger, M. Stolte, F. Würthner, H. Wadepohl, H. Klauk, L. H. Gade, *Adv. Funct. Mater.* **2013**, *23*, 3866–3874.

[35] L. Hahn, S. Öz, H. Wadepohl, L. H. Gade, *Chem. Commun.* **2014**, *50*, 4941–4943.

[36] L. Hahn, H. Wadepohl, L. H. Gade, *Org. Lett.* **2015**, *17*, 2266–2269.

[37] M. L. Tang, J. H. Oh, A. D. Reichardt, Z. Bao, *J. Am. Chem. Soc.* **2009**, *131*, 3733–3740.

[38] M. Winkler, K. N. Houk, *J. Am. Chem. Soc.* **2007**, *129*, 1805–1815.

[39] F. S. Tautz, S. Sloboshanin, J. A. Schaefer, R. Scholz, V. Shklover, M. Sokolowski, E. Umbach, *Phys. Rev. B* **2000**, *61*, 16933–16947.

[40] H. Ibach, D. Mills, *Electron Energy Loss Spectroscopy and Surface Vibrations*, Academic Press, New York, **1982**.

[41] C. Gahl, D. Brete, F. Leyssner, M. Koch, E. R. McNellis, J. Mielke, R. Carley, L. Grill, K. Reuter, P. Tegeder, *J. Am. Chem. Soc.* **2013**, *135*, 4273–4281.

[42] P. Navarro, F. C. Bocquet, I. Deperasińska, G. Pirug, F. S. Tautz, M. Orrit, *J. Phys. Chem. C* **2015**, *119*, 277–283.

[43] P. Tegeder, *J. Phys. Condens. Matter* **2012**, *24*, 394001.

[44] X. Zhan, A. Facchetti, S. Barlow, T. J. Marks, M. A. Ratner, M. R. Wasielewski, S. R. Marder, *Adv. Mater.* **2011**, *23*, 268–284.

[45] A. D. Becke, *J. Chem. Phys.* **1993**, *98*, 1372–1377.

[46] A. D. Becke, *J. Chem. Phys.* **1993**, *98*, 5648–5652.

[47] C. Lee, W. Yang, R. G. Parr, *Phys. Rev. B* **1988**, *37*, 785–789.

[48] F. Weigend, M. Häser, H. Patzelt, R. Ahlrichs, *Chem. Phys. Lett.* **1998**, *294*, 143–152.

[49] F. Weigend, R. Ahlrichs, *Phys. Chem. Chem. Phys.* **2005**, *7*, 3297–3305.

[50] F. Neese, *Wiley Interdiscip. Rev. Comput. Mol. Sci.* **2012**, *2*, 73–78.

[51] I. Seguy, P. Jolinat, P. Destruel, R. Mamy, H. Allouchi, C. Courseille, M. Cotrait, H. Bock, *ChemPhysChem* **2001**, *2*, 448–452.

[52] V. Shklover, F. S. Tautz, R. Scholz, S. Sloboshanin, M. Sokolowski, J. A. Schaefer, E. Umbach, *Surf. Sci.* **2000**, *454–456*, 60–66.

[53] M. Eremtchenko, D. Bauer, J. a. Schaefer, F. s. Tautz, *J. Mater. Res.* **2004**, *19*, 2028–2039.

[54] C. Bronner, F. Leyssner, S. Stremlau, M. Utecht, P. Saalfrank, T. Klamroth, P. Tegeder, *Phys. Rev. B* **2012**, *86*, 085444.

[55] C. Bronner, S. Stremlau, M. Gille, F. Brauße, A. Haase, S. Hecht, P. Tegeder, *Angew. Chem. Int. Ed.* **2013**, *52*, 4422–4425; *Angew. Chem.* **2013**, *125*, 4518–4521.

[56] S. M. Sze, K. K. Ng, *Physics of Semiconductor Devices*, Wiley, Hoboken, NJ, **2006**.

[57] J. Kirkpatrick, *Int. J. Quantum Chem.* **2008**, *108*, 51–56.

[58] Code: Https://code.google.com/p/j-Form-g03/.

[59] K. A. Peterson, D. Figgen, E. Goll, H. Stoll, M. Dolg, *J. Chem. Phys.* **2003**, *119*, 11113–11123.

[60] A. Klamt, G. Schüürmann, *J. Chem. Soc. Perkin Trans. 2* **1993**, 799–805.

[61] S. Sinnecker, A. Rajendran, A. Klamt, M. Diedenhofen, F. Neese, *J. Phys. Chem. A* **2006**, *110*, 2235–2245.

[62] Retrieved from http://www.chemcraftprog.com, **2015**.

[63] Gaussian 09, Revision B.01, M. J. Frisch, G. W. Trucks, H. B. Schlegel, G. E. Scuseria, M. A. Robb, J. R. Cheeseman, G. Scalmani, V. Barone, B. Mennucci, G. A. Petersson, H. Nakatsuji, M. Caricato, X. Li, H. P. Hratchian, A. F. Izmaylov, J. Bloino, G. Zheng, J. L. Sonnenberg, M. Hada, M. Ehara, K. Toyota, R. Fukuda, J. Hasegawa, M. Ishida, T. Nakajima, Y. Honda, O. Kitao, H. Nakai, T. Vreven, J. A. Montgomery, Jr., J. E. Peralta, F. Ogliaro, M. Bearpark, J. J. Heyd, E. Brothers, K. N. Kudin, V. N. Staroverov, R. Kobayashi, J. Normand, K. Raghavachari, A. Rendell, J. C. Burant, S. S. Iyengar, J. Tomasi, M. Cossi, N. Rega, J. M. Millam, M. Klene, J. E. Knox, J. B. Cross, V. Bakken, C. Adamo, J. Jaramillo, R. Gomperts, R. E. Stratmann, O. Yazyev, A. J. Austin, R. Cammi, C. Pomelli, J. W. Ochterski, R. L. Martin, K. Morokuma, V. G. Zakrzewski, G. A. Voth, P. Salvador, J. J. Dannenberg, S. Dapprich, A. D. Daniels, Ö. Farkas, J. B. Foresman, J. V. Ortiz, J. Cioslowski, D. J. Fox, Gaussian Inc., Wallingford, **2010**.

Contents:

SI.1 HREELS measurements:

Adsorption properties of TAPP derivatives

SI.1.1 Adsorption properties of TAPP-H

Table SI.1 contains the assignment of all observed vibrational modes shown in Fig. 3 of the main article.

Table SI.1: TAPP-H – Vibrational frequencies (in cm^{-1}) and assignments for 1 ML and 6 ML TAPP-H adsorbed on Au(111). *da* refers to dipole active modes. In addition DFT calculated frequencies based on the B3LYP functional and the 6-311G basis set of the free molecules are shown. υ, stretch; δ, in-plane bending; γ, out-of-plane bending; τ, torsion; in brackets: orientation of the calculated dipole derivative vector with respect to the molecular geometry, x long axis, y short axis, z perpendicular to the molecular plane).

HREELS monolayer cm^{-1}	HREELS multilayer cm^{-1}	DFT cm^{-1}	Displacement (DFT)
190	176	168	τ(C-C), short-axis buckling (x, z)
255	232	224	C-F$_2$-rocking (y)
-	290	282	τ(C-C), long-axis buckling + C-F$_2$-wagging (x, z)
523 (*da*)	526 (*da*)	493	δ(C-C-C) + δ(F-C-F) side chains (z)
581 (*da*)	607 (*da*)	612	δ(C-C-C) side chains (x, z)
734 (*da*)	704(*da*)	689	δ(C-C-C) (x, z)
	744 (*da*)	731	δ(C-C-C) + γ(N-C-N) (x, z)
806	802	767	γ(N-C-N) (x, z)
851 (*da*)	862 (*da*)	831	γ(C-H) (x, z)
911	-	866	γ(C-H) (x, z)
976 (*da*)	970 (*da*)	883	γ(C-H) (z)
1081	1062	1107	δ(F-C-F) side chains (x, z)
-	1117	1162	ν(C-F) (z)
1225 (*da*)	1241 (*da*)	1206	ν(C-F) (z)
1265 (*da*)	-	1241	ν(C-C) side chains + ν(C-F) (z)
1354	1349	1364	δ(C-C-C) side chains + δ(C-H) (x, z)
-	1527	1462	ν(C-C) + δ(N-C-N) (x)
-	1617	1562	ν(C-N) (x)
3057	3066	3258	ν(C-H) (y)

SI.1.2 Adsorption properties of TAPP-Cl

The coverage dependent adsorption geometries of TAPP-Cl are derived from the spectra shown in Figure SI.1 in a way analogous to the one shown in the main article for TAPP-H. The assignments of all vibrational modes are shown in Table SI.2. The C-N stretching modes ν(C-N) (Figure SI.1a)) are barely visible in the monolayer and dipole active in the multilayer (1463 and 1523 cm^{-1}, Figure SI.1b). The dynamic dipole moments of these vibrations are parallel to the long axis of the molecule (Table SI.2), so we can draw the conclusion, that the aromatic backbones of the molecules in the ML regime lie flat on the surface. In the multilayer they are tilted around their short axes, a finding which is supported by the reduced dipole activity and the reduced relative intensity of the out-of-plane C-H bending mode γ(C-H) in the multilayer (990 cm-1, Figure SI.1 b) compared to the monolayer (989 cm-1, Figure SI.1a). The tilting of the molecule is also tilting the dynamic dipole moment of the respective vibration and accordingly reducing the component perpendicular to the surface. These modes are reduced, compared to TAPP-H (Figure 3, main paper) due to the reduced number of hydrogen atoms in the molecule. For the same reason the C-H stretching mode ν(C-H) around 3000 cm^{-1} is not visible without magnification. However it is clear, that this mode is not dipole active. This indicates that its dynamic dipole moment which points parallel to the short axis of the molecule is compensated by the image dipole of the metal surface. The latter case results if the molecule is not tilted around its long axis in the mono- and multilayer regime. The different vibrational modes associated with the perfluorinated side chains are located in the same energy regime (1100 to 1400 cm^{-1}), thus precluding an unambiguous assignment. Geometrical arguments let us conclude that the side chains point upwards in the monolayer in order to reduce the distance between the aromatic molecular backbone and the metal surface allowing for increased attractive interactions. The spectra in Figure SI.1 show distinct differences between the mono- and the multilayer. We assign these differences to the different orientation of the side chains which changes the symmetry of the molecule from C_{2h} (both side chains point upwards) to C_{2v} (one side chain points upwards, one downwards). This change leads to a different dipole activity of the involved modes (ν(C-F) at 1222 cm-1 and 1200 cm-1 in Figure SI.1a and b respectively). So we conclude, that the molecules lie flat on the surface in the monolayer with both side chains pointing "upwards". With additional coverage the molecules adsorb in a tilted geometry with its side chains in opposite directions.
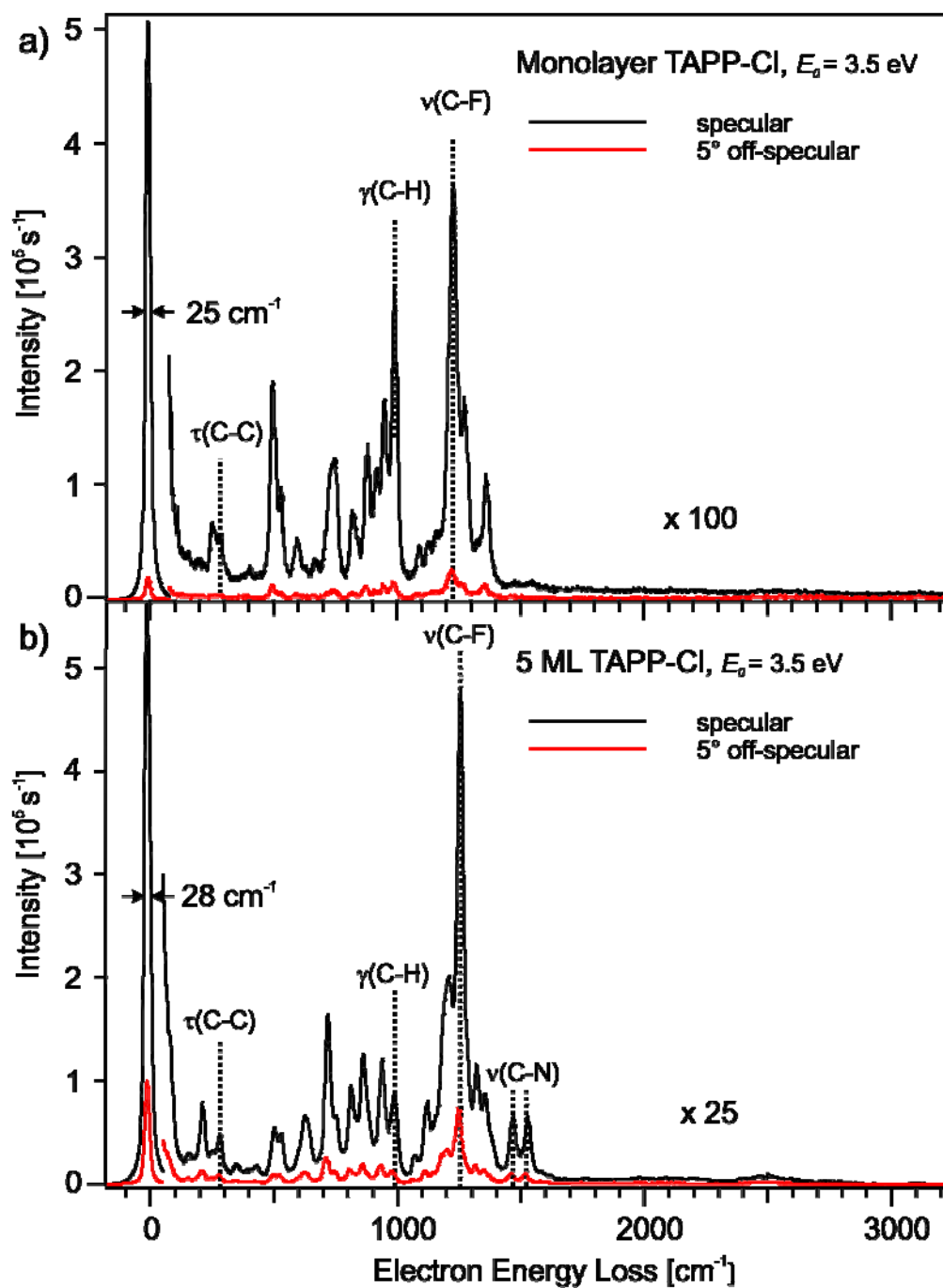
Figure SI.1: *Vibrational HREEL spectra in specular (black) and off-specular (red) scattering geometry for a TAPP-Cl monolayer (a) and a coverage of 5 ML TAPP-Cl (b) on the Au(111) surface. E_0 is the primary energy of the incident electrons. The energy resolution measured as FWHM of the elastic peak (zero loss peak) is 25/28 cm^{-1}.*

Table SI.2: TAPP-Cl – Vibrational frequencies (in cm^{-1}) and assignments for 1 ML and 5 ML TAPP-Cl adsorbed on Au(111). *da* refers to dipole active modes. In addition DFT calculated frequencies based on the B3LYP functional and the 6-311G basis set of the free molecules are shown. υ, stretch; δ, in-plane bending; γ, out-of-plane bending; τ, torsion; in brackets: orientation of the calculated dipole derivative vector with respect to the molecular geometry, x long axis, y short axis, z perpendicular to the molecular plane).

HREELS monolayer cm^{-1}	HREELS multilayer cm^{-1}	DFT cm^{-1}	Displacement (DFT)
-	167	157	τ(C-C), short-axis buckling (*x, z*)
257	221	210	C-F$_2$-rocking (*y*)
286	291	276	τ(C-C), long-axis buckling + C-F$_2$-wagging (*x, z*)
502 (*da*)	506	483	δ(C-C-C) + δ(F-C-F) side chains (*z*)
532	537	540	γ(C-H) (*x, z*)
600	635	613	δ(C-C-C) side chains (*x*)
741 (*da*)	721 (*da*)	685	γ(C-C-C) (*z*)
	750	720	δ(C-C-C) + γ(N-C-N) (*x, z*)
820	815	762	δ(C-C-C) + γ(N-C-N) (*x*)
879 (*da*)	865	825	γ(N-C-N) (*z*)
912	-	861	γ(N-C-N) + δ(C-H) (*x, z*)
940 (*da*)	941	919	γ(C-H) (*z*)
989 (*da*)	990	968	γ(C-H) (*z*)
1085	1069	1069	δ(F-C-F) side chains (*x, z*)
1131	1118	1122	υ(C-F) (*z*)
1222 (*da*)	1200	1165	υ(C-F) (*z*)
1277 (*da*)	1252 (*da*)	1218	υ(C-C) side-chains + υ(C-F) (*x, z*)
-	1319	1286	υ(C-C) side-chains (*x*)
1357	1355	1345	δ(C-C-C) side chains + δ(C-H) (*x, z*)
-	1463	1444	υ(C-C) + δ(N-C-N) (*x*)
-	1523	1543	υ(C-N) (*x*)

SI.1.3 Adsorption properties of TAPP-Br

In the following the coverage dependent adsorption geometries of TAPP-Br are derived from the spectra shown in Figure SI.2. The assignments of all vibrational modes are shown in Table SI.3. First of all a reduced intensity of the elastic peak and a really low dipole activity of the visible peaks are observed in the multilayer (Figure SI.2 b). This is in general a sign for a reduced ordering of the molecules compared to the monolayer. The C-N stretching modes ν(C-N) (Figure SI.2a)) are barely visible in the monolayer and dipole active in the multilayer (1457 and 1520 cm^{-1}, Figure SI.2b). The dynamic dipole moments of these vibrations are parallel to the long axis of the molecule (Table SI.3), so we can draw the conclusion, that the aromatic backbones of the molecules in the ML regime lie flat on the surface. In the multilayer they are tilted around their short axes, a finding which is supported by the reduced dipole activity and the reduced relative intensity of the out-of-plane C-H bending mode γ(C-H) in the multilayer (977 cm-1, Figure SI.2b) compared to the monolayer (974 cm-1, Figure SI.2 a). The tilting of the molecule is also tilting the dynamic dipole moment of the respective vibration and accordingly reducing the component perpendicular to the surface. As seen at TAPP-Cl, the relative intensities of these modes are reduced, compared to TAPP-H (Figure 3, main paper) due to the reduced number of hydrogen atoms in the molecule. For the same reason the C-H stretching mode γ(C-H) at 3086 cm^{-1} is only visible in the multilayer. The missing dipole activity of this mode indicates that its dynamic dipole moment which points parallel to the short axis of the molecule is compensated by the image dipole of the metal surface. The latter case results if the molecule is not tilted around its long axis in the mono- and multilayer regime. The different vibrational modes associated with the perfluorinated side chains are located in the same energy regime (1100 to 1400 cm^{-1}), thus precluding an unambiguous assignment. Geometrical arguments let us conclude that the side chains point upwards in the monolayer in order to reduce the distance between the aromatic molecular backbone and the metal surface allowing for increased attractive interactions. The spectra in Figure SI.2 show distinct differences between the mono- and the multilayer. We assign these differences to the different orientation of the side chains which changes the symmetry of the molecule from C_{2h} (both side chains point upwards) to C_{2v} (one side chain points upwards, one downwards). This change leads to a different dipole activity of the involved modes (ν(C-F) at 1226 cm^{-1} and 1159/1251 cm^{-1} in Figure SI.2a and b respectively). So we conclude, that the molecules lie flat on the surface in the monolayer with both side chains pointing "upwards". With additional coverage the molecules adsorb in a tilted geometry with its side chains in opposite directions. As mentioned at the beginning, the multilayer shows less ordering than the monolayer and the TAPP-Cl and TAPP-H multilayers. This is probably due to the bigger bromine atoms compared to chlorine or even hydrogen which inhibit a nice packing above the first layer.

Figure SI.2: *Vibrational HREEL spectra in specular (black) and off-specular (red) scattering geometry for a TAPP-Br monolayer (a) and a coverage of 5 ML TAPP-Br (b) on the Au(111) surface. E_0 is the primary energy of the incident electrons. The energy resolution measured as FWHM of the elastic peak (zero loss peak) is 28/30 cm^{-1}.*

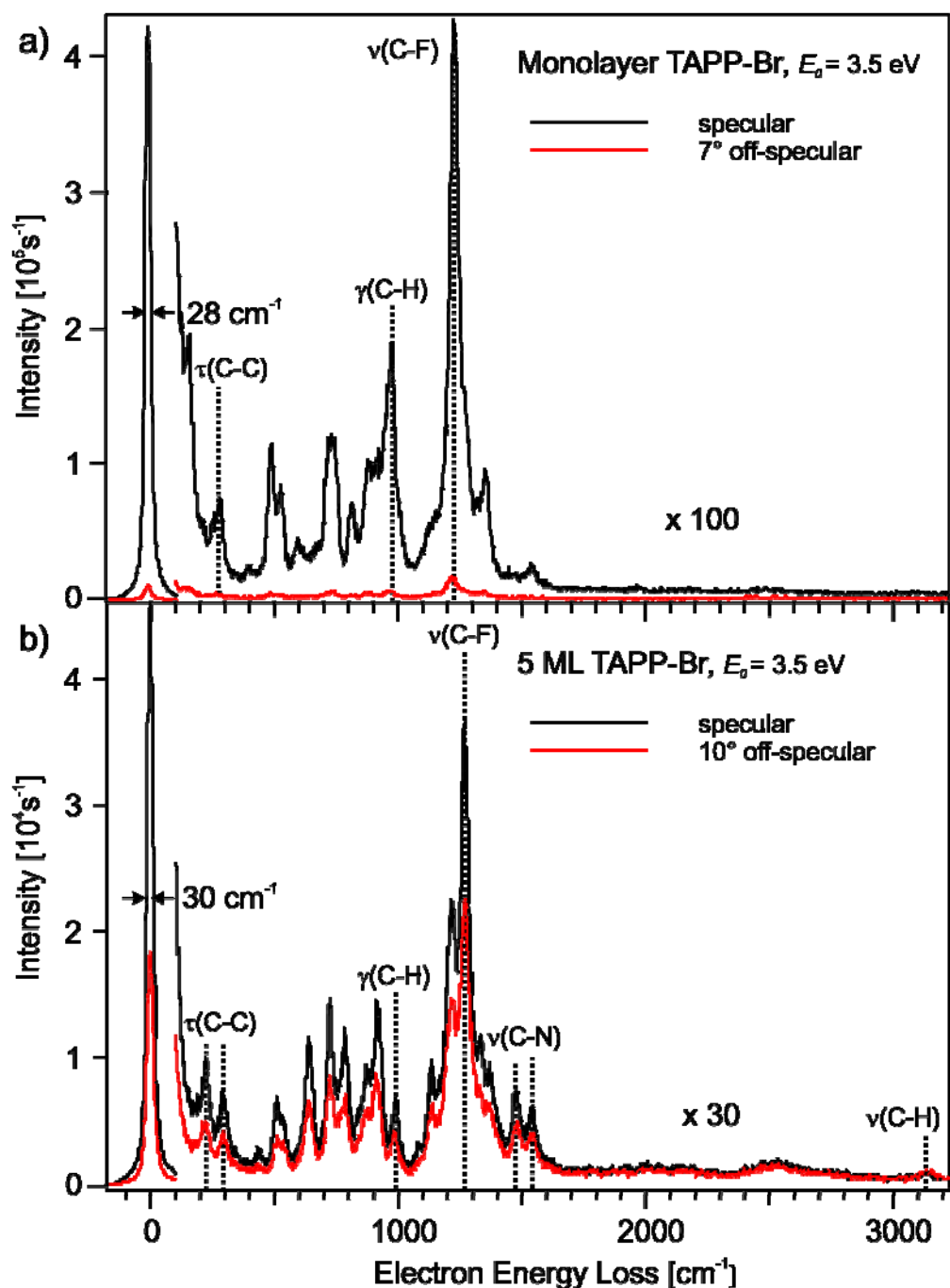**Table SI.3:** TAPP-Br – Vibrational frequencies (in cm^{-1}) and assignments for 1 ML and 5 ML TAPP-Br adsorbed on Au(111). *da* refers to dipole active modes. In addition DFT calculated frequencies based on the B3LYP functional and the 6-311G basis set of the free molecules are shown. υ, stretch; δ, in-plane bending; γ, out-of-plane bending; τ, torsion; in brackets: orientation of the calculated dipole derivative vector with respect to the molecular geometry, *x* long axis, *y* short axis, *z* perpendicular to the molecular plane).

HREELS monolayer cm^{-1}	HREELS multilayer cm^{-1}	DFT cm^{-1}	Displacement (DFT)
167	-	168	τ(C-C), short-axis buckling (*x, z*)
224	220	203	C-F$_2$-rocking (*y*)
288	289	274	τ(C-C), long-axis buckling (*x*)
492 (*da*)	501	484	δ(C-C-C) + δ(F-C-F) side chains (*z*)
535	532	564	γ(C-H) (*x, z*)
601	633 (*da*)	619	δ(C-C-C) side chains (*x*)
736 (*da*)	715 (*da*)	680	δ(C-C-C) (*x, z*)
	777	744	δ(C-C-C) + γ(N-C-N) (*x, z*)
815	-	775	γ(N-C-N) (*z*)
881	859	851	γ(N-C-N) (*x, z*)
924	907 (*da*)	934	γ(C-H) (*z*)
974 (*da*)	977	952	γ(C-H) (*z*)
	1067	1070	δ(F-C-F) side chains (*x, z*)
1127	1117	1122	υ(C-F) (*z*)
1226 (*da*)	1195 (*da*)	1195	υ(C-F) (*z*)
	1251 (*da*)	1251	υ(C-C) side chains + υ(C-F) (*z*)
1354	1354	1345	δ(C-C-C) side chains + δ(C-H) (*x, z*)
-	1457	1442	υ(C-C) + δ(N-C-N) (*x*)
1537	1520	1538	υ(C-N) (*x*)
-	3086	3241	υ(C-H) (*y*)

SI.1.4 Adsorption properties of TAPP-I

In the following the coverage dependent adsorption geometries of TAPP-I are derived from the spectra shown in Figure SI.3. The assignments of all vibrational modes are shown in Table SI.4. First of all a strongly reduced intensity of the elastic peak is observed in the multilayer (Figure SI.3b). This is in general a sign for a reduced ordering of the molecules compared to the monolayer. It needs to be mentioned that the monolayer is only well ordered when the sample is not annealed to more than 400 K. Hence it was not possible to get well defined monolayers by removing the multilayer by heating to 450 K. The monolayer underlying the spectrum in Figure SI.3a was obtained by direct dosing. Additional dosing immediately lead to a strong reduction of the intensity of the elastic peak. The C-N stretching modes ν(C-N) are only barely visible in the monolayer (1457 and 1531 cm^{-1}, Figure SI.3a) and appear as a broad shoulder in the multilayer (1463 and 1525 cm^{-1}, Figure SI.3b). The dynamic dipole moments of these vibrations are parallel to the long axis of the molecule (Table SI.4), so we can draw the conclusion, that the aromatic backbones of the molecules in the ML regime lie flat on the surface. The relative intensity of the out-of-plane C-H bending mode γ(C-H) in the multilayer (982 cm^{-1}, Figure SI.3b) compared to the monolayer (977 cm^{-1}, Figure SI.3a) is reduced. This is probably caused by a tilting of the molecule which is also tilting the dynamic dipole moment of the respective vibration and accordingly reducing the component perpendicular to the surface. The C-H stretching mode ν(C-H) at 3092 cm^{-1} is only visible in the multilayer. Due to the quality of the multilayer spectra it is hard to say something about the dipole activity of this mode. The different vibrational modes associated with the perfluorinated side chains are located in the same energy regime (1100 to 1400 cm^{-1}, broad peaks at 1234 cm^{-1} and 1219 cm^{-1} in Figure SI.3a and b respectively), thus precluding an unambiguous assignment. So we conclude, that the molecules in the monolayer lie flat and well-ordered on the surface with both side chains pointing "upwards". With additional coverage the ordering is strongly reduced, probably because of the huge iodine atoms which inhibit a nice packing above the first layer.
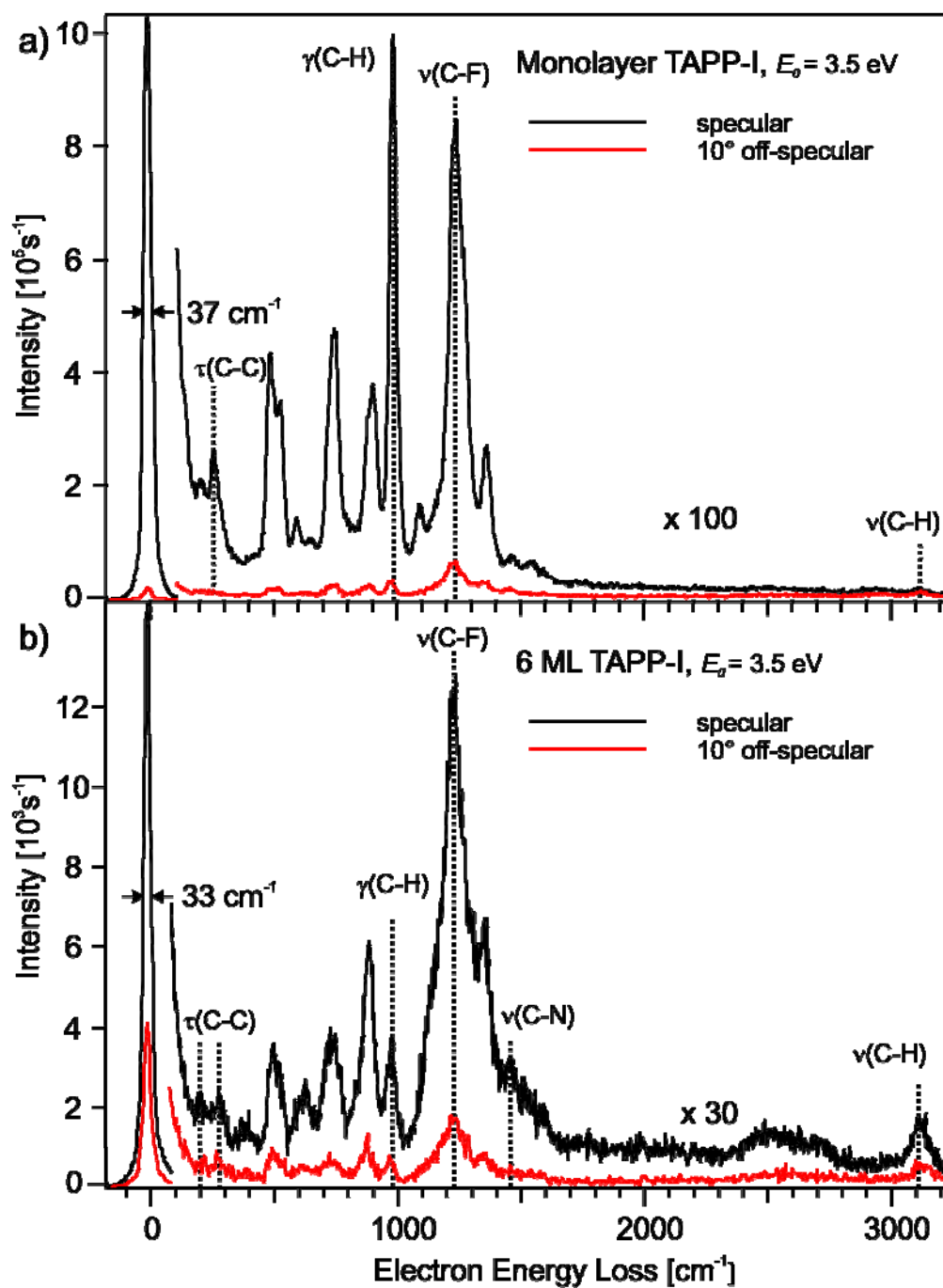
Figure SI.3: *Vibrational HREEL spectra in specular (black) and off-specular (red) scattering geometry for a TAPP-I monolayer (a) and a coverage of 6 ML TAPP-I (b) on the Au(111) surface. E_0 is the primary energy of the incident electrons. The energy resolution measured as FWHM of the elastic peak (zero loss peak) is 30/33 cm^{-1}.*

Table SI.4: TAPP-I – Vibrational frequencies (in cm^{-1}) and assignments for 1 ML and 6 ML TAPP-I adsorbed on Au(111). *da* refers to dipole active modes. In addition DFT calculated frequencies based on the B3LYP functional and the LANL2DZ basis set of the free molecules are shown. υ, stretch; δ, in-plane bending; γ, out-of-plane bending; τ, torsion; in brackets: orientation of the calculated dipole derivative vector with respect to the molecular geometry, *x* long axis, *y* short axis, *z* perpendicular to the molecular plane).

HREELS monolayer cm^{-1}	HREELS multilayer cm^{-1}	DFT cm^{-1}	Displacement (DFT)
211	211	202	C-F$_2$-rocking (*y, z*)
262	285	267	τ(C-C), long-axis buckling (*x, z*)
488 (*da*)	506 (*da*)	476	δ(C-C-C) + δ(F-C-F) side chains (*z*)
530		541	γ(C-H) (*x, z*)
598	630	608	δ(C-C-C) side chains (*x*)
747 (*da*)	735 (*da*)	741	γ(C-C-C) + δ(C-C-C) (*x, z*)
902 (*da*)	881 (*da*)	896	γ(N-C-N) + γ(C-H) (*x, z*)
982 (*da*)	977 (*da*)	950	γ(C-H) (*z*)
1086	-	1064	δ(F-C-F) side chains (*x, z*)
1234 (*da*)	1219 (*da*)	1152	υ(C-F) (*z*)
1351	1348	1336	δ(C-C-C) side chains + δ(C-H) (*x, z*)
1457	1463	1483	υ(C-C) + δ(N-C-N) (*x*)
1531	1525	1537	υ(C-N) (*x*)
3077	3092	3265	υ(C-H) (*y*)

SI.2: Solid state UV/Vis absorption spectra of TAPP-H and TAPP-Hal.
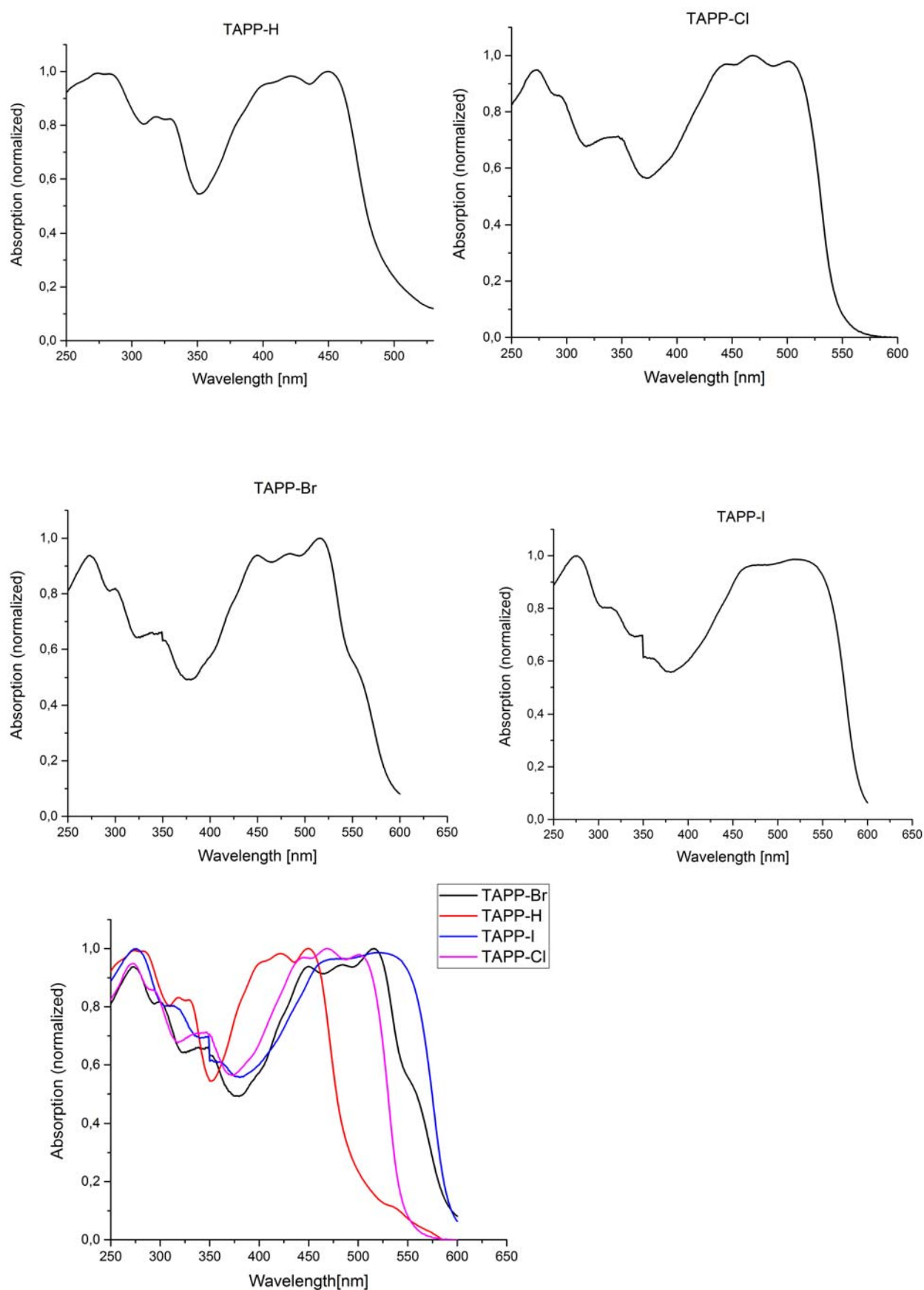
Figure SI.4: solid state UV/Vis absorption spectra of TAPP-H and TAPP-Hal.

SI. 3 DFT Modeling

Coordinates of the optimized structures:

42

TAPP-H

C	5.37992380906180	-0.01669681450139	0.57123819819463
C	3.47425954024078	-1.23870874585638	0.33435606968384
C	2.72190436758449	-0.03438559871309	0.25335529221809
C	3.45764299904020	1.18090602344297	0.33936008803580
C	2.76967441670442	-2.48642905792102	0.24536535622428
C	1.30300946342256	-0.04350095356512	0.09271276436265
C	0.62223962736694	-1.29974350142402	0.01328186037389
C	1.41110649753722	-2.50336403246665	0.09465423008711
C	-0.79653226123896	-1.30896073192584	-0.14417705093592
C	-1.49417094201465	-0.06187872159160	-0.21866979905888
C	-0.81340221232775	1.19436579656409	-0.13924028134260
C	0.60537135824146	1.20358256129025	0.01821913221050
C	1.37777013784088	2.41795289896830	0.10419523324609
C	2.73599963568593	2.41928397948533	0.25505541051394
H	0.86483202602801	3.37767371315922	0.04503584745404
H	0.91113396859620	-3.46972364336413	0.03188254540088
C	-2.91306941308321	-0.07099860265424	-0.37928158387403
C	-3.66543351754562	1.13331819928044	-0.46027270657855
C	-3.64880332947308	-1.28629262546908	-0.46526415992328
N	-5.00159720936766	1.10853608558032	-0.61877737476857
N	-4.98282541002198	-1.27904084035994	-0.62389765589702
N	4.79166559630517	1.17364926713673	0.49804427679394
N	4.81042666803269	-1.21393737054815	0.49289569910384
C	-5.57108925101992	-0.08870371198693	-0.69708915903509
C	-2.96084955294090	2.38103742454581	-0.37128098350373
C	-1.60227922368609	2.39798308020267	-0.22059534050072
H	-1.10231321715169	3.36434678881558	-0.15781071053294
C	-1.56892591112532	-2.52333296141930	-0.23013311262337
H	-1.05598262213339	-3.48304861865153	-0.17096770480169
C	-2.92715636581498	-2.52466561208049	-0.38096014446171
C	-7.09813214067842	-0.12488579241207	-0.82848807376637
C	6.90695434009636	0.01946865972522	0.70276044223576
F	-7.59676738284492	1.05382485265263	-1.20084682216125
F	-7.49109657132809	-1.04149810073585	-1.72422463075604
F	7.29983883935579	0.93596219335213	1.59865911109376
F	7.40554991431364	-1.15930267512915	1.07498920527341
H	-3.49864406619742	-3.45214466104274	-0.44624360226399
H	-3.54374093940002	3.30160337503261	-0.43260246165697
H	3.30753650893505	3.34684360002267	0.32036880450121
H	3.35265052502817	-3.40714887081950	0.30672569951869
F	7.45630674992906	0.34128462521674	-0.48166760623245
F	-7.64738144995274	-0.44653587983548	0.35603369814882

42

TAPP-H radical anion

C	5.39681136118566	-0.01702159715898	0.57499313379730
C	3.49086189009427	-1.24571528450742	0.34115972796598
C	2.73893234738074	-0.03395089003232	0.25936176945970
C	3.47427664809883	1.18832597222840	0.34593654898564
C	2.78907818081439	-2.47493068832086	0.25431106004418
C	1.31650274407294	-0.04331201010102	0.09682027708336
C	0.63466589184255	-1.30244038162251	0.01674029893930
C	1.41398117887136	-2.48660246288264	0.09996254005910
C	-0.80848146753143	-1.31196931988664	-0.14664496331795
C	-1.50765331791606	-0.06206190310904	-0.22277484104598
C	-0.82582007833959	1.19706854341565	-0.14269448817119
C	0.61733135303720	1.20659534832499	0.02068308198265
C	1.38046774147449	2.40119714732661	0.10758528635916
C	2.75517161277608	2.40824009331977	0.26254901990916
H	0.86767138471024	3.36251343449610	0.04832668881032
H	0.91419199063800	-3.45457752765473	0.03808186740125
C	-2.93008695537497	-0.07143174628446	-0.38528187221137
C	-3.68203165242645	1.14032657398707	-0.46705806845738
C	-3.66542423388450	-1.29371381938902	-0.47185550771765
N	-5.03515374134561	1.11306042390223	-0.62625654621909
N	-5.01643096489166	-1.28348338208873	-0.63214570526031
N	4.82527827723334	1.17808379307412	0.50628594271652
N	4.84397678443413	-1.21846025980350	0.50040665933108
C	-5.58798059568236	-0.08838533871115	-0.70082099985525
C	-2.98024802982449	2.36954459008829	-0.38020686259355
C	-1.60514616057448	2.38122799357552	-0.22589207405918
H	-1.10536500268009	3.34920730962466	-0.16400393472401
C	-1.57160809769283	-2.50657549816112	-0.23354974926161
H	-1.05880442147987	-3.46788776247473	-0.17429970885283
C	-2.94631254516381	-2.51362398747138	-0.38848994403874
C	-7.11251623133256	-0.12432038310143	-0.82470472797350
C	6.92133577132405	0.01888527448296	0.69899144661999
F	-7.63253731506543	1.05419800280852	-1.18987801353285
F	-7.52671979871905	-1.03653560996792	-1.72462331145993
F	7.33547945819643	0.93098906358715	1.59905373704111
F	7.44130545402509	-1.15969020145275	1.06405595830576
H	-3.51024322317427	-3.44624382519429	-0.45513673533902
H	-3.55621945661429	3.29504723951320	-0.44346657521753
H	3.31910749909096	3.34085751626368	0.32920141157143
H	3.36503893975157	-3.40043874202797	0.31760040956679
F	7.48692964533381	0.34741590412365	-0.48323777605905
F	-7.67800886467234	-0.45271660273794	0.35761353941818

42

TAPP-F

C	5.38967374527750	-0.01487516497210	0.55802306224504
C	3.48034957573124	-1.22732917620040	0.37197647089351
C	2.71507298796704	-0.03213784233914	0.27620236996689
C	3.46513579543210	1.17454237529549	0.36989624716911
C	2.75673099718339	-2.47071992053868	0.32542479809920
C	1.29739839751437	-0.04231687467200	0.10754205639113
C	0.62168603617860	-1.30175610033287	0.02979033809067
C	1.40222661254212	-2.50293442368617	0.15085917202540
C	-0.79544430571174	-1.31227128788967	-0.15333266212774
C	-1.48844953996726	-0.06305440936555	-0.23459086660453
C	-0.81272978022513	1.19638847012176	-0.15697406536970
C	0.60440952513052	1.20690408895505	0.02618735885602
C	1.36840807856405	2.41970778265960	0.14489937265413
C	2.72291495026931	2.40752912968761	0.32131555768261
H	0.88083969140875	3.39357905312549	0.10813864284257
H	0.92862169741251	-3.48372100157562	0.11705666330293
C	-2.90617680959762	-0.07324575287416	-0.40276083956042
C	-3.67148486963636	1.12193814724060	-0.49830213158982
C	-3.65628585783051	-1.27993162357223	-0.49604338322309
N	-5.00473435240258	1.10460911378125	-0.63240885791611
N	-4.98792811268953	-1.27997143165133	-0.63022019437241
N	4.79669946687086	1.17457139040700	0.50497146100951
N	4.81351517962117	-1.21001337528106	0.50688187869690
C	-5.58093920155088	-0.09052897618460	-0.68296239305143
C	-2.94786230341899	2.36536447914787	-0.45219072187915
C	-1.59328685502300	2.39756760527242	-0.27800887996395
H	-1.11965428983969	3.37834642475070	-0.24437403620301
C	-1.55946556083971	-2.52507751013577	-0.27187370570621
H	-1.07187954648993	-3.49894456006103	-0.23524404475508
C	-2.91403698137356	-2.51292206419988	-0.44780759268440
C	-7.11161640959565	-0.12189452926294	-0.77140316494052
C	6.92026321366908	0.01645409693570	0.64792999314134
F	-7.61141969444255	1.07596447502960	-1.07034820878365
F	-7.52400166789084	-0.99413055480820	-1.70028043118712
F	7.33178269163496	0.88830855364176	1.57753354479085
F	7.41973898840409	-1.18153989899314	0.94687863991372
F	-3.59133907972457	-3.64551329044032	-0.58501621300276
F	-3.64082109058878	3.48840554761405	-0.58891902842129
F	3.40018418034628	3.54015204905686	0.45880910427342
F	3.44968326993555	-3.59386405646063	0.46226057824916
F	7.43750423202078	0.39902627768897	-0.53050566399846
F	-7.62767900427541	-0.50397023491430	0.40768777504677

42

TAPP-F radical anion

C	5.40690008989900	-0.01527541163093	0.55849502527554
C	3.49770699931596	-1.23411144693835	0.37055591580822
C	2.73326807611876	-0.03165313524679	0.27318570821993
C	3.48261959868713	1.18169291027806	0.36708962565838
C	2.77602359561870	-2.45368652974006	0.32639305545912
C	1.31149567632586	-0.04210277829671	0.10692857961324
C	0.63277134529927	-1.30331450715615	0.03270652866631
C	1.40678866813747	-2.48654155025763	0.15436829762654
C	-0.80620288134486	-1.31410868894104	-0.15202160488389
C	-1.50276055412084	-0.06327571017470	-0.23192293706765
C	-0.82404672699864	1.19793725771821	-0.15762528192164
C	0.61493287011683	1.20872876429283	0.02707016330356
C	1.37278106923018	2.40327499784917	0.14437622710049
C	2.74204953047755	2.39080477697300	0.31835104225020
H	0.88802423659875	3.37944157684165	0.10756945207834
H	0.93579627819608	-3.46948705232555	0.12257164462551
C	-2.92449276995863	-0.07372627422008	-0.39850524760653
C	-3.68890991504381	1.12872941410932	-0.49609299737125
C	-3.67379552670877	-1.28707422282394	-0.49275561027757
N	-5.04059743722326	1.10966691930415	-0.63360352192147
N	-5.02395306063123	-1.28509638712871	-0.63197020895076
N	4.83283811500171	1.17970903622750	0.50579689713419
N	4.84944870820611	-1.21505561327228	0.50758015442417
C	-5.59800271396810	-0.09011847073156	-0.68476654660265
C	-2.96723997993354	2.34830454810615	-0.45177750334830
C	-1.59803756185477	2.38116475432759	-0.27949324213284
H	-1.12704015687219	3.36410799979486	-0.24771489450077
C	-1.56401059667667	-2.50865531434411	-0.26960281985330
H	-1.07924537985916	-3.48481870952880	-0.23284265984953
C	-2.93323391990378	-2.49617954297771	-0.44391569658331
C	-7.12544345011379	-0.12127505437653	-0.77811315219157
C	6.93442512028415	0.01583994430491	0.65084663726008
F	-7.64450828900956	1.07791938517331	-1.06422896442354
F	-7.55146373955958	-0.98073359264235	-1.72143265371163
F	7.36114942633698	0.87545431353539	1.59370819621783
F	7.45361398421906	-1.18332303727879	0.93686117287238
F	-3.59739096815143	-3.65532899315001	-0.57796879624755
F	-3.64783719394309	3.49760309136442	-0.58741485357045
F	3.40625924585044	3.54997151750187	0.45200079935786
F	3.45666257798698	-3.60299732194716	0.46171287351011
F	7.47568370392380	0.41445710688822	-0.51868475822820
F	-7.66742209395512	-0.52017396946066	0.39098395478241

42

TAPP-Cl

C	5.38454395162289	-0.01693449716369	0.57813644638899

42

TAPP-Cl radical anion

C	5.40076798909358	-0.01732190884564	0.58209647221135

C 3.48304204523055   -1.23701329872378   0.33310186279270
C 2.72097739112876   -0.03480662101790   0.25324543390708
C 3.46619017412647   1.17855821166296   0.33894496505297
C 2.76074393678054   -2.48590125017572   0.23059659507697
C 1.30320932957944   -0.04380300130603   0.09227878041575
C 0.62288024033210   -1.29633277165515   0.01139175547798
C 1.39952554591359   -2.49816548633050   0.08247287758790
C -0.79741678284448   -1.30547204777589   -0.14298379220487
C -1.49450985070930   -0.06191621690539   -0.21710171911470
C -0.81416716133016   1.19058529373533   -0.13631233270714
C 0.60611114803810   1.19970799398019   0.01787116457154
C 1.36613833667165   2.41213743531145   0.09476099422635
C 2.72692995595939   2.41815117405583   0.24273468011480
H 0.86610012173390   3.37669466460058   0.02975426304088
H 0.91251364077673   -3.46907155161438   0.01238340698276
C -2.91223658022394   -0.07078903120600   -0.37820148289565
C -3.67415524278940   1.13151261386057   -0.45779289707490
C -3.65751953998383   -1.28404454507195   -0.46469413607998
N -5.00394315152151   1.10648536389386   -0.61978533415453
N -4.98518450299248   -1.27605685142769   -0.62693925687373
N 4.79391886514329   1.17078819867058   0.50071926544429
N 4.81284710279385   -1.21177423207759   0.49526600608158
C -5.57571850180038   -0.08821510008964   -0.70332568784439
C -2.95179934969795   2.38035412385907   -0.35592554557781
C -1.59059881157049   2.39250141179210   -0.20788699113260
H -1.10345255993236   3.36339708671159   -0.13866854733875
C -1.55749899523687   -2.51784613902248   -0.22085381847487
H -1.05752087493703   -3.48249420758347   -0.15671459666333
C -2.91825409353204   -2.52371183107579   -0.36930039775165
C -7.10329899996255   -0.12396648967618   -0.84212650888512
C 6.91227933618548   0.01923912465341   0.71605876628663
F -7.59644858676552   1.05398018344989   -1.21957669166747
F -7.48953571264683   -1.04256144018054   -1.73682574328457
F 7.29222084649221   0.94162444708571   1.60649505057054
F 7.40553839648855   -1.15702020069669   1.09857902391085
Cl -3.77801040020036   -4.02038110402567   -0.44470069684581
Cl -3.83022737226441   3.86672030799671   -0.42301040710226
Cl 3.58665692526423   3.91491608228920   0.31626439991826
Cl 3.63930371694141   -3.97229104042911   0.29619928888875
F 7.46171948165751   0.33209931536772   -0.46961997674776
F -7.65329341791878   -0.44218407774549   0.34179353368431

C 3.49970296569459   -1.24375020810573   0.34055374342948
C 2.73742752349610   -0.03432215219290   0.25990254532612
C 3.48306134573841   1.18566847955624   0.34618046281884
C 2.77688644559449   -2.46747374993879   0.23961984086554
C 1.31659410094186   -0.04345590625529   0.09628472909558
C 0.63398732893389   -1.29791505440669   0.01367257574520
C 1.40232649993688   -2.48253103808203   0.08645720968371
C -0.80794651912157   -1.30733147403228   -0.16644382268818
C -1.50771049963772   -0.06189689907751   -0.22292112771030
C -0.82508446801503   1.19255888780859   -0.14048248462315
C 0.61686170600985   1.20196365798141   0.01933039229741
C 1.36907575911481   2.39680754587338   0.09702866590620
C 2.74330372722662   2.40016718512569   0.25028621499335
H 0.87267464262529   3.36390098174442   0.03186959646153
H 0.91884758286296   -3.45586298489700   0.01715296467115
C -2.92858649383634   -0.07101310336567   -0.38603561842766
C -3.69096386685519   1.13840694298539   -0.46583476332885
C -3.67415595087342   -1.29099119280926   -0.47275931913918
N -5.03729249117129   1.11128035437424   -0.62755070469177
N -5.01829283703108   -1.28079391658091   -0.63557902412137
N 4.82715014326345   1.17550398286173   0.50955757872052
N 4.84590206355728   -1.21658224203431   0.50347590729723
C -5.59207826783709   -0.08796084993829   -0.70651351450412
C -2.96806462544428   2.36209774898914   -0.36556830488369
C -1.59342507346804   2.37716760311731   -0.21317744698469
H -1.10988845501436   3.35051085598258   -0.14438864823026
C -1.56009848950101   -2.50219694855930   -0.22482020891062
H -1.06365313811348   -3.46930607651827   -0.16038726417889
C -2.93432612838525   -2.50552821232543   -0.37800182690139
C -7.11761739552554   -0.12395814955332   -0.83592937899034
C 6.92628851509485   0.01848336682033   0.71272790080159
F -7.63166811604328   1.05318561984791   -1.20707507758948
F -7.52473193645689   -1.03934069236738   -1.73303026270396
F 7.33301033237403   0.93597929712680   1.60788482029780
F 7.43945099735735   -1.15790969633929   1.08742483602436
Cl -3.77702882272072   -4.03192488681497   -0.45426017886519
Cl -3.82994359632514   3.87819230216936   -0.43401864708307
Cl 3.58603017709068   3.92661041883382   0.32546963514791
Cl 3.63872514565556   -3.98361628817321   0.30793898262011
F 7.49033795649778   0.33852775671521   -0.47068521263070
F -7.68025577678358   -0.44732935670005   0.34724976277185

42

TAPP-Br

C 5.38539999698905   -0.01715508652942   0.58087006328020
C 3.48468219572462   -1.23865884739559   0.32428484618588
C 2.72273471573342   -0.03493239808762   0.24793520007470
C 3.46756883197413   1.17988730868504   0.33201426337309
C 2.76336498895927   -2.48621757424880   0.21226515341643

42

TAPP-Br radical anion

C 5.40198092561326   -0.01749277936631   0.58475526475620
C 3.50141612666761   -1.24536624753424   0.33511915948772
C 2.73857826839265   -0.03472358080437   0.25796713985086
C 3.48429504155806   1.18655317215428   0.34253950853884
C 2.77841824372792   -2.46765951438851   0.22569285867919

```
C   1.30452442931592   -0.04380113304072    0.08893013324674        C   1.31757242450871   -0.04371555762168    0.09544007937404
C   0.62352974267644   -1.29581016373455    0.00751420650364        C   0.63451073855634   -1.29774604324647    0.01149676446038
C   1.40173283663060   -2.49833449579639    0.06968353522729        C   1.40364623701822   -2.48319752783043    0.07640968871150
C  -0.79785303512037   -1.30483838990627   -0.14174907551814        C  -0.80856779515435   -1.30704027463264   -0.14506432884838
C  -1.49571817190459   -0.06168733301650   -0.21436248160780        C  -1.50872649065296   -0.06184588363612   -0.22112214538833
C  -0.81471137970333    1.19030119569531   -0.13287079587864        C  -0.82567517963947    1.19217467337958   -0.13699026083146
C   0.60665011727801    1.19933092622642    0.01633940955348        C   0.61740023501904    1.20146086476350    0.01934292409665
C   1.36819789149448    2.41242741132474    0.08588879187056        C   1.37026757954452    2.39719047020550    0.09057589822867
C   2.72944675253188    2.41842873721839    0.22752079114320        C   2.74472108790533    2.39990727566469    0.23929536347166
H   0.86246789381011    3.37362666648495    0.01559669055174        H   0.86848352098898    3.36101482040266    0.02021436157537
H   0.90890026252090   -3.46579239865269   -0.00713574007440        H   0.91470054137249   -3.45321379833766    0.00048545655625
C  -2.91391067993489   -0.07048804378525   -0.37356267623182        C  -2.92971495910733   -0.07077934203881   -0.38375282907023
C  -3.67583482413623    1.13326313180510   -0.44997661536105        C  -3.69251574104518    1.13988497623953   -0.46065173260756
C  -3.65874990223596   -1.28527142724961   -0.45792642275155        C  -3.67547593361113   -1.29199645636600   -0.46861221728046
N  -5.00518857169749    1.10602212869845   -0.61713714252939        N  -5.03770524012243    1.11067155990571   -0.62686766886024
N  -4.98592813644010   -1.27513933470753   -0.62507548334697        N  -5.01841538155198   -1.27960496534389   -0.63558323432605
N   4.79477061303201    1.16981491200520    0.49889619785665        N   4.82725365228425    1.17426163712998    0.50926374614505
N   4.81406311454731   -1.21134550935471    0.49121919138385        N   4.84664528674993   -1.21602650139694    0.50110760391747
C  -5.57653334543445   -0.08815399310289   -0.70703064900142        C  -5.59307443021472   -0.08780620099117   -0.71095127556638
C  -2.95447108033138    2.38077163510311   -0.33775273443056        C  -2.96956027168241    2.36212385502080   -0.35071253649523
C  -1.59286255358110    2.39283614085475   -0.19504230800665        C  -1.59479515215234    2.37765031925246   -0.20152850913110
H  -1.10003530712138    3.36028600785340   -0.11809575066483        H  -1.10587772808280    3.34765464473899   -0.12532412787414
C  -1.55944335257297   -2.51790534905897   -0.21160766354040        C  -1.56148858506981   -2.50273798002535   -0.21660493701809
H  -1.05373791612999   -3.47912790052235   -0.14144716957920        H  -1.05972383244274   -3.46658911077637   -0.14640805715445
C  -2.92067627415671   -2.52384885238061   -0.35351811926349        C  -2.93594860497686   -2.50539306318359   -0.36544587569848
C  -7.10331105120222   -0.12458288820339   -0.85861823808307        C  -7.11815083489457   -0.12427638151917   -0.85072208266629
C   6.91218125174800    0.01929922885960    0.73224054944052        C   6.92709145940602    0.01922329332131    0.72408224725990
F  -7.59257795086982    1.04806051752120   -1.25688238859533        F  -7.62838834304745    1.04872577302691   -1.23884940713888
F  -7.48264159189042   -1.05426464489653   -1.74444468047315        F  -7.51912567822013   -1.04884956923293   -1.74045786813459
F   7.29148585448805    0.94817122207860    1.61894125623475        F   7.32812271020793    0.94368892413862    1.61390658623027
F   7.40159866935616   -1.15370377167182    1.12925572965823        F   7.43772356686069   -1.15373342838340    1.11181396899024
Br -3.85675252901517   -4.16121049497463   -0.40683774319592        Br -3.85517597877274   -4.17127661870411   -0.42194730454854
Br -3.91046055528924    4.00698798829077   -0.38247548417205        Br -3.90872123719240    4.01713767410588   -0.39940191910624
Br  3.66541818265160    4.05583806370049    0.27991561051171        Br  3.66371359988643    4.06589962170031    0.29537337389037
Br  3.71957373150686   -4.11236149816131    0.25706247976464        Br  3.71737934272803   -4.12282588091660    0.27555781675827
F   7.47206431746187    0.32233526012482   -0.45109361249233        F   7.49644156331748    0.32945730203344   -0.45918672333226
F  -7.66335818166288   -0.42635695405221    0.32497087552087        F  -7.68793475468011   -0.43408415090739    0.33244723009847
```

42   42

TAPP-I   **TAPP-I radical anion**

```
C   5.38653635900105   -0.01683146636136    0.57918600128132        C   5.40405373460483   -0.01706263212615    0.58168718709999
C   3.48304362677074   -1.24003145206542    0.33614050042539        C   3.50084679323882   -1.24587065281725    0.34377413147381
C   2.72235239227388   -0.03439746598128    0.25595287599362        C   2.73838185378063   -0.03401472861959    0.26277035405911
C   3.46628059486193    1.18231302305080    0.34226949777820        C   3.48405990434560    1.18850043904582    0.34999281188810
C   2.76541311867435   -2.48978609802289    0.23570431758072        C   2.78005215783595   -2.46958698937343    0.24601096911380
C   1.30424543582002   -0.04345158879326    0.09360888354560        C   1.31742116058326   -0.04327360251222    0.09831505163904
C   0.62382804358111   -1.29655388127510    0.01208985734074        C   0.63506450275019   -1.29857654916529    0.01564405633684
C   1.40376446129796   -2.50024391322254    0.08594721223551        C   1.40516360432454   -2.48536637760278    0.09172980003477
C  -0.79792292289208   -1.30580460101347   -0.14514782455566        C  -0.80879921950281   -1.30811253768928   -0.14739542857520
```

16

C	-1.49529376717204	-0.06181175135210	-0.22054562682671	C	-1.50848318373196	-0.06197931985418	-0.22503067933630
C	-0.81487236062034	1.19129803871682	-0.13904344501318	C	-0.82612990451911	1.19333654414756	-0.14242026095682
C	0.60688582615165	1.20055252412685	0.01816459373235	C	0.61775183451800	1.20287605182780	0.02070658974635
C	1.37025279210976	2.41487970988220	0.09761375565924	C	1.37155128472278	2.39999791561920	0.10153618844538
C	2.73144346965289	2.42287457404397	0.24759506521582	C	2.74607031774864	2.40300408111275	0.25666341288347
H	0.85586422831508	3.37189104303929	0.03129522952920	H	0.86159731902592	3.35990941669840	0.03597775214657
H	0.90226875360345	-3.46380059019433	0.01512829510480	H	0.90809938254238	-3.45177842345952	0.02276376407595
C	-2.91344243108705	-0.07090942074307	-0.38252783914028	C	-2.92948108685427	-0.07129972841286	-0.38919303188370
C	-3.67424466103291	1.13468956114391	-0.46238586182249	C	-3.69201776817628	1.14051392609667	-0.47013294190198
C	-3.65732920773091	-1.28765133619731	-0.46863468052946	C	-3.67515239009689	-1.29385049051168	-0.47600114611232
N	-5.00458970778207	1.10443484503290	-0.62275700878002	N	-5.03727226136464	1.10855724124272	-0.62993608979861
N	-4.98563650005831	-1.27457672227732	-0.62918894825530	N	-5.01832370028684	-1.27883590549228	-0.63704266016163
N	4.79451487359534	1.16917270988562	0.50337601815709	N	4.82717068473676	1.17339817853746	0.51160607556377
N	4.81330918661387	-1.20983098884410	0.49712401759602	N	4.84604036166619	-1.21399731990194	0.50397099147256
C	-5.57777397841349	-0.08863155730452	-0.70463479668970	C	-5.59528085115690	-0.08842590784775	-0.70720259084064
C	-2.95657959161442	2.38444666614018	-0.36204797227513	C	-2.97121837385739	2.36426127914774	-0.37255012032831
C	-1.59489067560591	2.39496350381270	-0.21266317112054	C	-1.59629469489439	2.38009969195946	-0.21846763046357
H	-1.09343217429732	3.35853083665790	-0.14175870242512	H	-1.09927399306529	3.34653811540411	-0.14951985579245
C	-1.56124750009294	-2.52015873968133	-0.22441277665667	C	-1.56257192601017	-2.50525718500604	-0.22793260530205
H	-1.04683021479496	-3.47714834178176	-0.15800507135860	H	-1.05259035674695	-3.46514642492836	-0.16229454808437
C	-2.92246855367973	-2.52820164908504	-0.37409561864423	C	-2.93712022379981	-2.50831715765349	-0.38268862435768
C	-7.10583106479193	-0.12430385062547	-0.83830878674654	C	-7.12133260289992	-0.12379510385092	-0.83271680080473
C	6.91447873032689	0.01864249375664	0.71415517515564	C	6.93000754188679	0.01812943367263	0.70820868472348
F	-7.59950957560242	1.05322406623106	-1.21630807941607	F	-7.63353425745697	1.05425787506598	-1.20134587316324
F	-7.49517756521552	-1.04441433089816	-1.72995717691346	F	-7.52935127743599	-1.03823826371784	-1.72943986734610
F	7.30301064926257	0.93807417714500	1.60692775714922	F	7.33746735912821	0.93161881373819	1.60616200702252
F	7.40763755813385	-1.15925712829775	1.09170942970668	F	7.44188520195836	-1.16037070357944	1.07588536172175
I	-3.97679471713863	-4.35560373695894	-0.46529052567196	I	-3.97617015983047	-4.35982242164033	-0.47852688077914
I	-4.03398569562200	4.19904827894191	-0.44427312345140	I	-4.03424642351808	4.20270491084951	-0.46093277568424
I	3.78575524162880	4.25026488805670	0.33937101992244	I	3.78510852240615	4.25448348205116	0.35320328788521
I	3.84270974241256	-4.30440947682008	0.31861487714810	I	3.84299081048363	-4.30806889761002	0.33464596115893
F	7.46178342372845	0.33528670570071	-0.47126011174201	F	7.48873217921231	0.34336764474981	-0.47547232879161
F	-7.65192264257125	-0.44007755756857	0.34796876777685	F	-7.67926885629485	-0.44780771759434	0.35168430197334

SI.4 Transfer Integrals.

In order to calculate the transfer integrals two neighbouring molecules of one π-stack were taken from the crystallographic data and are referred to as A and B. Transfer integrals were calculated using the following equation:

$$t = J^{eff} = \frac{J_{AB} - \frac{1}{2}(e_A + e_B)S_{AB}}{1 - S_{AB}^2}$$

$$J_{AB} = <\phi^A | \hat{H} | \phi^B > \quad S_{AB} = <\phi^A | \phi^B >$$

$$e_A = <\phi^A | \hat{H} | \phi^A > \quad e_B = <\phi^B | \hat{H} | \phi^B >$$

SI.5 X-ray Crystal Structure Determinations

Crystal data and details of the structure determinations are compiled in Table **S1**. Full shells of intensity data were collected at low temperature with a Agilent Technologies Supernova-E CCD diffractometer (Mo- or Cu-K_α radiation, microfocus X-ray tube, multilayer mirror optics). Data were corrected for air and detector absorption, Lorentz and polarization effects;[#1] absorption by the crystal was treated analytically[#1,#2] or with a semiempirical multiscan method.[#3,#4] The structures were solved by the charge flip procedure[#5] (**TAPP-F·2CDCl₃**) or by the heavy atom method combined with structure expansion by direct methods applied to difference structure factors[#6] (**TAPP-I**) and refined by full-matrix least squares methods based on F^2 against all unique reflections.[#7] All non-hydrogen atoms were given anisotropic displacement parameters. Hydrogen atoms were input at calculated positions and refined with a riding model.

CCDC 406814-1406815 contains the supplementary crystallographic data for this paper. These data can be obtained free of charge from The Cambridge Crystallographic Data Centre via www.ccdc.cam.ac.uk/data_request/cif.

References

#1   *CrysAlisPro*, Agilent Technologies UK Ltd., Oxford, UK **2011-2014**.

#2   R. C. Clark, J. S. Reid, *Acta Cryst.* **1995**, *A51*, 887;

#3   R. H. Blessing, *Acta Cryst.* **1995**, *A51*, 33.

#4   (a) G. M. Sheldrick, *SADABS*, Bruker AXS GmbH, Karlsruhe, Germany **2004-2014**; (b) L. Krause, R. Herbst-Irmer, G. M. Sheldrick, D. Stalke, *J. Appl. Cryst.* **2015**, *48*, 3.

#5   (a) L. Palatinus, *SUPERFLIP*, EPF Lausanne, Switzerland and Fyzikální ústav AV ČR, v. v. i., Prague, Czech Republic, **2007-2014**; (b) L. Palatinus, G. Chapuis, *J. Appl. Cryst.* **2007**, 40, 786.

#6   (a) P. T. Beurskens, G. Beurskens, R. de Gelder, J. M. M. Smits, S. Garcia-Granda, R. O. Gould, *DIRDIF-2008*, Radboud University Nijmegen, The Netherlands, **2008**; (b) P. T. Beurskens, in: G. M. Sheldrick, C. Krüger, R. Goddard (eds.), *Crystallographic Computing 3*, Clarendon Press, Oxford, UK, **1985**, p. 216.

#7   (a) G. M. Sheldrick, *SHELXL-20xx*, University of Göttingen and Bruker AXS GmbH, Karlsruhe, Germany **2012-2014**; (b) G. M. Sheldrick, *Acta Cryst.* **2008**, *A64*, 112; (c) G. M. Sheldrick, *Acta Cryst.* **2015**, *C71*, 3.

Table S1. Details of the crystal structure determinations of **TAPP-F·2CDCl₃** and **TAPP-I**.

	TAPP-F·2CDCl₃	TAPP-I
Formula	$C_{30}H_4Cl_6D_2F_{18}N_4$	$C_{28}H_4F_{14}I_4N_4$
crystal system	monoclinic	triclinic
space group	$P\,2_1/c$	P -1
a /Å	10.1702(3)	5.0400(6)
b /Å	10.1392(3)	10.5468(13)
c /Å	16.4662(5)	14.3120(19)
α /°		106.013(11)
β /°	94.768(3)	94.290(10)
γ /°		91.147(10)
V /Å³	1692.07(8)	728.54(16)
Z	2	1
M_r	979.10	1169.95
F_{000}	956	538
d_c /Mg·m⁻³	1.922	2.667
μ /mm⁻¹	0.641	34.725
max., min. transmission factors	0.983, 0.907	1.0000, 0.5093
X-radiation, λ /Å	Mo-$K\alpha$, 0.71073	Cu-$K\alpha$, 1.54184
data collect. temperat. /K	110(1)	110(1)
θ range /°	3.3 to 32.4	4.4 to 70.1
index ranges (indep. set) h,k,l	-15 ... 15, -15 ... 15, -24 ... 24	-6 ... 6, -12 ... 12, -17 ... 16
reflections measured	51795	9037
unique [R_{int}]	5845 [0.0681]	2576 [0.0744]
observed [$I{\geq}2\sigma(I)$]	4260	2166
data / restraints /parameters	5845 / 0 / 262	2576 / 84 / 226
GooF on F^2	1.035	1.117
R indices [$F>4\sigma(F)$] $R(F)$, $wR(F^2)$	0.0533, 0.1089	0.1091, 0.2667
R indices (all data) $R(F)$, $wR(F^2)$	0.0827, 0.1205	0.1230, 0.2775
largest residual peaks /e·Å⁻³	0.799, -0.623	3.645, -1.256